ORIGINAL ARTICLE

Decreased *LDHB* expression in breast tumor cells causes NK cell activation and promotes tumor progression

Zhihong Luo[1,2], Xiaohua Huang[1], Xinyi Xu[1], Kefeng Wei[1], Yi Zheng[3], Ke Gong[4], Wenhua Li[1,2]

[1]Hubei Key Laboratory of Cell Homeostasis, College of Life Sciences, Wuhan University, Wuhan 430072, China; [2]Wuhan University Shenzhen Research Institute, Shenzhen 518057, China; [3]Central Laboratory, University of Chinese Academy of Sciences-Shenzhen Hospital, Shenzhen 518107, China; [4]Hubei Province Key Laboratory of Allergy and Immunology and Department of Immunology, School of Basic Medical Sciences, Wuhan University, Wuhan 430071, China

ABSTRACT

Objective: Abnormal metabolism is the underlying reason for breast cancer progression. Decreased lactate dehydrogenase B (*LDHB*) has been detected in breast cancer but the function of *LDHB* remains unknown.

Methods: Western blot was used to analyze *LDHB* expression in breast cancer cells. The impact of *LDHB* on tumor cell migration and invasion was determined using Transwell assays, wound healing assays, and a mouse lung metastasis model. Subcutaneous tumor formation, a natural killer (NK) cell cytotoxicity assay, and flow cytometry evaluated NK cell activation. Immunofluorescence and quantitative real-time PCR detected NK cell activation markers. Kaplan-Meier analysis evaluated the effect of immune cell infiltration on prognosis. Single-sample gene set enrichment analysis determined NK cell activation scores. A support vector machine predicted the role of *LDHB* in NK cell activation.

Results: In this study we showed that *LDHB* inhibits the breast cancer cell metastasis and orchestrates metabolic reprogramming within tumor cells. Our results revealed that *LDHB*-mediated lactic acid clearance in breast cancer cells triggers NK cell activation within the tumor microenvironment. Our findings, which were confirmed in a murine model, demonstrated that *LDHB* in tumor cells promotes NK cell activation and ultimately results in the eradication of malignant cells. Clinically, our study further validated that *LDHB* affects immune cell infiltration and function. Specifically, its expression has been linked to enhanced NK cell-mediated cytotoxicity and improved patient survival. Furthermore, we identified *LDHB* expression in tumors as an important predictor of NK cell activation, with strong predictive ability in some cancers.

Conclusions: Our results suggest that *LDHB* is a promising target for activating the tumor immune microenvironment in breast cancer, where *LDHB*-associated lactic acid clearance leads to increased NK cell activity. This study highlights the critical role of *LDHB* in regulating immune responses and its potential as a therapeutic target for breast cancer.

KEYWORDS   Breast cancer; lactate dehydrogenase B; lactic acid; NK cells; tumor immunity

Introduction

Breast cancer (BRCA) is the most common and fatal tumor affecting women[1]. The tumor microenvironment (TME) comprises a complex interplay of diverse cellular and non-cellular components that exert a pivotal influence on BRCA progression[2,3]. The emergence and progression of tumors frequently involve evasion of immune surveillance and destruction by immune cells, including T and natural killer (NK) cells, within the TME[4]. Tumor cells within solid tumors recruit immunosuppressive cells, such as myeloid-derived suppressor cells (MDSCs), type 2 macrophages (M2), and regulatory T cells (Tregs), by secreting chemokines[5,6]. In addition, tumor cells possess the unique ability to exploit nutrients and secrete metabolites, thereby effectively modulating the TME. By orchestrating this complex interaction, tumor cells establish an immunosuppressive milieu that fuels tumor progression and facilitates metastasis[7,8]. Recently, although immunotherapy using checkpoint inhibitors has shown significant clinical success[9] some patients may still exhibit a poor response or treatment failure[10,11]. BRCA is a malignant tumor with poor immunogenicity, forming an "immune-cold" tumor

2

Luo et al. Diminished *LDHB* in breast tumors impedes NK cells

immune microenvironment[12,13], which results in insensitivity to immunotherapy[14,15]. Therefore, understanding the state of immune cells in the tumor can provide theoretical guidance for clinical immunotherapy.

NK cells, an important immune component of the TME, are cytotoxic lymphocytes that can effectively eliminate diverse tumor cells and modulate adaptive immune responses by releasing cytokines[16,17]. NK cells are activated after the integration of signals originating from activating receptors on target cells and inhibitory receptors that engage MHC I molecules[18,19]. However, tumor-infiltrating NK cells often exhibit a dysfunctional phenotype, contain fewer activating receptors and more inhibitory receptors, and interferon-gamma (IFN-γ) secretion is reduced[20]. An abundance of evidence has emerged over the past few years confirming that tumor metabolites are central to many aspects of NK cell biology[21-23]. However, the mechanisms by which these metabolites modulate NK cell function are poorly understood.

Metabolic reprogramming, a hallmark of tumors[24], is characterized by the preferential metabolism of glucose to lactic acid *via* glycolysis. This process enables tumor cells to rapidly generate ATP and glycolytic intermediates, thereby supporting high tumor cell proliferation rates. This phenomenon, commonly referred to as the Warburg effect or aerobic glycolysis, is a key factor that drives tumor growth and survival[25,26]. Lactate dehydrogenase B (*LDHB*) is a critical subunit of lactate dehydrogenase that is responsible for catalyzing the conversion of lactic acid to pyruvate *via* the glycolytic pathway[27]. *LDHB* has a crucial role in extracellular and intracellular lactic acid removal[28,29], thereby supporting oxidation during the tricarboxylic acid cycle (TCA) and exhibiting a reverse Warburg effect in tumor cells[30]. A recent study demonstrated that double knockout of *LDHA* and *LDHB* may be necessary to completely inhibit glycolysis in cancer cells[31]. *LDHB* is thought to be an essential gene in triple-negative BRCA but is downregulated in HER2+ and luminal BRCA cells[32]. In addition, *LDHB* expression is suppressed under hypoxic conditions[33]. Although *LDHB* is essential for most metabolic events, the functional consequences of *LDHB* in BRCA and the relevance in priming NK cell activity within the TME are currently unknown.

In this study we assessed the immune profiles of patients with BRCA using data from The Cancer Genome Atlas (TCGA). We demonstrated the critical function of *LDHB* in stimulating NK cell-mediated tumor eradication by decreasing lactic acid levels in the TME. Moreover, our results showed that BRCA patients with high *LDHB* expression exhibit enhanced NK cell cytotoxicity, leading to improved patient survival.

Material and methods

Data collection

TCGA transcriptome profiling data were downloaded from https://portal.gdc.cancer.gov/. TCGA patient clinical information was simultaneously obtained. The single-cell RNA sequencing data used in this study were obtained from the Gene Expression Omnibus (GEO) database under the accession number, GSE180286.

Cell lines

The mouse mammary carcinoma cell line, 4T1, was obtained from the CCTCC (Wuhan, China). Human BRCA cell lines (MDA-MB-231, T-47D, MCF-7, ZR-75-30, and BT-549) and the normal mammary epithelial cell (MCF10A) were purchased from the ATCC (Manassas, VA, USA). MCF10A was cultured in a growth medium comprised of DMEM/F12 (Gibco, Grand Island, NY, USA) supplemented with 5% horse serum, 20 ng/mL of epidermal growth factor (EGF), 10 μg/mL of insulin, 0.5 μg/mL of hydrocortisone, 100 ng/mL of cholera toxin, and 1% penicillin-streptomycin (Beyotime, Shanghai, China). Other cell lines were maintained in Dulbecco's modified Eagle's medium (DMEM; Gibco) supplemented with 10% fetal bovine serum (AusGeneX, Molendinar, QLD, Australia) and 1% penicillin-streptomycin. All cells were cultured at a controlled temperature of 37°C in a humidified incubator with 5% CO_2.

To establish the 4T1-*Ldhb* and BT-549-*LDHB* cell lines, a lentiviral vector carrying *Ldhb* or *LDHB* was stably transfected into cells. Following transfection, the cells were subjected to puromycin selection to obtain a stable cell line expressing *Ldhb*. As a control, the cells were transfected with an empty vector (4T1-Vector and BT-549-Vector).

Human BRCA samples

BRCA tumor samples were collected from consented patients during surgery at the University of Chinese Academy of Sciences-Shenzhen Hospital (Guangming, China). High-throughput RNA sequencing (RNA-seq) was performed to capture the transcriptome by Benagen (Wuhan, China). The

sequencing data underwent quality control, alignment to the reference genome, and quantification of gene expression levels. This study was approved by the Ethics Committee of the the University of Chinese Academy of Sciences-Shenzhen Hospital (Approval No. LL-KT-2022086). The processed transcriptome data is available in **Table S2**.

Identification of differentially expressed genes and functional enrichment analysis

We excluded the healthy group and patients without survival information, and stratified breast cancer patients into *LDHB*-low and *LDHB*-high groups based on the level of *LDHB* gene expression. Differential expression analysis between these groups was performed using the R package (edgeR) with a significance threshold of $P < 0.05$ and an absolute |Log2[fold change (FC)] | >1.45. The biological functions of the differentially expressed genes (DEGs) were then assessed using hypergeometric enrichment analysis, which included Gene Ontology (GO) and Kyoto Encyclopedia of Genes and Genomes (KEGG) analyses. The ClusterProfiler package was used for functional annotation analysis, with a significance threshold P-value cut-off = 0.01 and a q-value cut-off = 0.05[34].

To identify significantly different biological processes between the *LDHB*-low and *LDHB*-high groups, we performed gene set enrichment analysis (GSEA) using version 4.1.0 software. The reference set used was "c2.cp.kegg.v2022.1.Hs. symbols" from the Molecular Signature Database [MSigDB (https://www.gsea-msigdb.org/gsea/msigdb)], and gene set permutations with 1,000 times were conducted to achieve a normalized enrichment score for each analysis. A false discovery rate < 0.05 was considered significant enrichment.

Immune cell infiltration and function estimation

We utilized the xCell algorithm (https://xcell.ucsf.edu/) to assess immune cell infiltration in the *LDHB*-low and *LDHB*-high groups[35]. Activation of NK cells in BRCA patients was quantified using single sample gene set enrichment analysis (ssGSEA) *via* the R package, GSVA[36]. The MSigDB "GOBP positive regulation of natural killer cell activation" gene set was used as the reference set to evaluate NK cell activation.

We calculated the effects of the immune cell infiltration score on overall survival (OS) in the high and low *LDHB* groups. Kaplan-Meier (KM) survival curves with a log-rank

P-value and hazard ratios (HRs) were generated using the R packages, survminer and survival.

Single-cell RNA sequencing data analysis

Single-cell RNA sequencing data from GSE180286 was used in this study to analyze primary BRCA samples from five patients. Raw count data were processed using R software and the Harmony package was used to correct batch effects and integrate the datasets. The integrated data were then visualized using Uniform Manifold Approximation and Projection (UMAP) analysis, with filtering parameters set to min.cells = 5 and min.features = 500, and cells with a percent_mito > 15% were excluded.

To annotate cell types, we utilized the "HumanPrimaryCellAtlasData" dataset in the SingleR package, which assigns cell types based on reference gene expression profiles.

Construction of the classification model by SVM

To predict NK cell killing activity, an initial support vector machine (SVM) model was trained using the level of *LDHB* expression in BRCA, liver cancer (LIHC), and pancreatic cancer (PAAD). The e1071 package was used to perform 10-fold cross-validation during the training of the SVM model[37], which is a supervised classification algorithm in machine learning. The diagnostic efficacy of the model was estimated using receiver operating characteristic (ROC) curves and the area under the ROC curve (AUC) with the pROC package.

Isolation and culture of NK cells

We purified primary NK cells that were identified by the marker, $CD3^-CD49b^+$, from the spleens of 6-week-old male BALB/c mice using flow cytometry. The mice were sacrificed and the spleens were digested in 5 mL of collagenase III (C8490; Solarbio, Beijing, China) for 60 min in a shaking bed at 37°C, followed by filtration through a 300-mesh filter membrane. We then added 3 mL of red blood cell lysis buffer [C3702 (500 mL); Beyotime, Shanghai, China], centrifuged the cells at 750 g for 5 min at 4°C, and washed the cells with PBS. The cell suspension were resuspended in 100 μL of PBS and a small number of cells were used to establish blank and single control groups for each fluorescent dye to obtain fluorescence complementary data. We added

4

Luo et al. Diminished *LDHB* in breast tumors impedes NK cells

CD3 (100203; BioLegend, San Diego, CA, USA) and CD49b (108921; BioLegend) fluorescent antibodies (15 µL each) to the experimental group, incubated the cells in the dark for 30 min, washed the cells with PBS, and centrifuged at 750 g for 5 min at 4°C and removed the supernatant. Finally, we added a specified volume of NK cell culture medium based on the cell number, resuspended the cells in a 15-mL centrifuge tube, and sorted the NK cells by flow cytometry (Sony MA900; Tokyo, Japan). The isolated NK cells were cultured in RPMI-1640 (31800-022; Thermo Fisher Scientific, Waltham, MA, USA) supplemented with 10% FBS (FBSCN500-S; AusGeneX, Molendinar, QLD, Australia), 100 units/mL of penicillin and 100 mg/mL streptomycin (C0222; Beyotime), $1 \times$ L-glutamine, and 100 U/mL recombinant mouse IL-2 (CM003-20MP; Chamot Biotechnology, Shanghai, China).

Wound healing assay

The cells were enzymatically dissociated, counted, and seeded at a density of 3×10^5 cells per well in a 12-well plate. Upon achieving confluence, a straight line was marked on the adherent cells from top-to-bottom using a 200-µL pipette tip. The cells were thrice-washed with 1 mL of PBS and replenished with an additional 1 mL of PBS. Subsequently, the cells were cultured in serum-free DMEM (12800-017; Thermo Fisher Scientific) in an incubator at 37°C in 5% CO_2. Images were acquired at 12 and 24 h post-wounding. The scratch closure rate was calculated as follows: (initial scratch area - residual scratch area)/initial scratch area × 100%.

Transwell assay

Cells were trypsinized and resuspended in a serum-free medium in preparation for the Transwell migration assay. Then, the cells in the upper chamber were gently removed with cotton swabs. Three random fields of view were chosen for image capture.

Animal experiments

All animal protocols were approved by the Animal Care and Use Committee of the College of Life Science (Wuhan University, Wuhan, China) and were in compliance with the National Research Council Guide for the Care and Use of Laboratory Animals. BALB/c female mice (6–8 weeks old, weighing 18–24 g; Shulaibao Biotech, Wuhan, China), immunodeficient NOD-SCID mice ($Prkdc^{-/-}$, 6 weeks old; Cyagen Biosciences, Suzhou, China), and NSG mice ($Prkdc^{-/-}$ IL2rg$^{-/-}$, 6 weeks old; Cyagen Biosciences) were housed in standard cages at 22–24°C with a 12 h:12 h light/dark cycle and had access to water *ad libitum*. The subcutaneous tumor formation mouse models were established by injecting a 200-µL 4T1-Vector or 4T1-*Ldhb* cell suspension (1×10^5) into each BALB/c, NOD-SCID, and NSG mouse. Mice were monitored every other day for weight and tumor volume, which was calculated using the formula, $0.5 \times$ length $\times$ width^2. The experiment was terminated and the mice were euthanized when the tumor volume reached a diameter of approximately 15 mm.

Control or 4T1-*Ldhb*-Luciferase cells (1×10^5 in 100 µL) were injected intravenously into the tail veins of mice to establish the BALB/c mouse pulmonary metastasis model. Live imaging was subsequently performed 4 weeks post-injection to assess pulmonary metastases.

Flow cytometry and sorting

To obtain single-cell suspensions of tumor-infiltrating immune cells, we utilized mechanical dissociation and collagenase digestion, followed by resuspension in staining buffer (PBS with 1% FBS and 2 mM EDTA). The cells were then stained with the following antibodies, as indicated: FITC anti-mouse CD3 (100203; BioLegend); PE/Cyanine7 anti-mouse CD49b (108921; BioLegend); APC anti-mouse CD8a (100711; BioLegend); Pacific Blue anti-mouse CD4 (100534; BioLegend); and PE anti-mouse Ifng (505807; BioLegend). The samples were analyzed by flow cytometry (CytoFLEX; Beckman, Brea, CA, USA) and flow analyses were performed using FlowJo 10.6.1 software.

NK cell cytotoxicity

NK cells were isolated from the spleens of BALB/c mice and pre-activated in 4T1-Vector CM or 4T1-*Ldhb* CM at 37°C with 5% CO_2 for 17 h supplemented with rIL-2 (1,000 U/mL). Target 4T1 cells were labeled with 200 nM MitoTracker® Green FM (40742ES50; Yeasen, Shanghai, China) at 37°C with 5% CO_2 for 20 min. Co-cultures were prepared with 3×10^4 target cells and varying effector-to-target (E: T) ratios (e.g., E:T of 5 with 1.5 $\times 10^5$ effector cells) in 300 µL of 4T1-Vector CM or 4T1-*Ldhb* CM along with rIL-2 (1,000 U/mL). These co-cultures were initiated in the presence or absence of 10 mM lactic acid in the culture medium. Subsequently, the cells were incubated at 37°C

in an atmosphere containing 5% CO_2 for a duration of 4 h. Cell lysis was assessed by adding propidium iodide (PI, 556547; BD Pharmingen, San Diego, CA, USA), followed by a 30-min incubation in the dark. After centrifugation, cells were resuspended in PBS, filtered, and analyzed using flow cytometry.

Immunohistochemistry and laser confocal microscopy experiment

Immunohistochemistry (IHC) was performed using mouse tumor tissues to detect CD8$^+$ and CD4$^+$ T cells using APC anti-mouse CD8a (100711; BioLegend) and Pacific Blue anti-mouse CD4 antibodies (100534; BioLegend), respectively. Tissue fluorescence confocal microscopy was performed using PE anti-mouse Ifng (505807; BioLegend), PE/Cyanine7 anti-mouse CD49b (108921; BioLegend), and DAPI staining for nuclear detection. Immunofluorescence staining of breast cancer patient tissues using antibodies obtained from Servicebio (Wuhan, China). Tissue sectioning and staining were performed by Servicebio and imaging was performed using a Leica laser scanning confocal microscope (Wetzlar, Germany).

Metabolite extraction and analysis

Metabolites from 4T1-Vector and 4T1-*LDHB* cells were extracted following established protocols[38]. High-resolution metabolite analysis was performed using the TripleTOF™ 6600+ mass spectrometer (Sciex, Framingham, MA, USA). Raw data were rigorously processed and analyzed using the MetDNA2 platform (http://metdna.zhulab.cn/). MetaboAnalyst (https://www.metaboanalyst.ca/) was used for comprehensive downstream analysis and data interpretation. The processed metabolomic dataset is presented in **Table S1**.

Quantitative real-time PCR

RNA was extracted using the standard TRIzol RNA extraction protocol (R401-01; Vazyme, Nanjing, China) for RT-PCR. Complementary DNA was performed using a High-capacity cDNA Reverse Transcription kit (11123ES60; Yeason) according to the manufacturer's instructions. Quantitative RT-PCR was performed using Hieff qPCR SYBR Green PCR Master Mix (11202ES08; Yeason) and gene-specific primers. *GAPDH* was used as a housekeeping gene and relative quantification was calculated as $2^{-\Delta\Delta CT}$. The primer pairs were as follows: *Ldhb*, 5-CCTCAGATCGTCAAGTACAGCC-3 (forward) and 5-ATCCGCTTCCAATCACACGGTG-3 (reverse); *Mct1*, 5-GACCATTGTGGAATGCTGCCCT-3 (forward) and 5-CGATGATGAGGATCACGCCACA-3 (reverse); *Mct4*, 5-GATGCCTCCTACCTTGTGTCTG-3 (forward) and 5-GCAAGCAGGTTAGTCACACCAC-3 (reverse); *Ifng*, 5-CAGCAACAGCAAGGCGAAAAAGG-3 (forward) and 5-TTTCCGCTTCCTGAGGCTGGAT-3 (reverse); *Gzmb*, 5-CAGGAGAAGACCCAGCAAGTCA-3 (forward) and 5-CTCACAGCTCTAGTCCTCTTGG-3 (reverse); and *Gapdh* 5-CATCACTGCCACCCAGAAGACTG-3 (forward) and 5-ATGCCAGTGAGCTTCCCGTTCAG-3 (reverse).

Glucose absorption and lactic acid concentration detection

Cells were cultured in glucose-free DMEM for 1 h to assay glucose uptake. Next, 2-NBDG (11046; Cayman Chemical, Ann Arbor, MI, USA) was added at a final concentration of 5 μM for 30 min. Cells were then washed with PBS and subjected to fluorescence-activated cell sorting (FACS) detection.

To determine lactic acid concentrations, 10^6 cells were seeded in a 6-well plate and allowed to grow for 12 h. Next, the cell culture supernatants were harvested and lactic acid was quantified using the L-Lactate Assay Kit 1 (A019-2-1; Nanjing Jiancheng, Nanjing, China).

Flow cytometric assessment of intracellular reactive oxygen species (ROS)

Cells were collected into 1.5-mL EP tubes and centrifuged at 400 g for 5 min at room temperature. After discarding the supernatant, cells were resuspended in 1 mL of serum-free DMEM culture medium. Subsequently, a 10 μM final concentration of the C400 probe (Thermo Fisher Scientific), a carboxylated H2DCFDA analog, was gently pipetted into the cell suspension, followed by a 30-min incubation at 37°C in the dark. After centrifugation and resuspension in PBS buffer, flow cytometry-specific tubes were employed to transfer the cell suspension for intracellular ROS assessment using a flow cytometer.

NAD$^+$:NADH ratio detection

For the NAD$^+$:NADH ratio determination, 1×10^6 cells were harvested, and after removing the culture medium, 200 μL of

6

Luo et al. Diminished *LDHB* in breast tumors impedes NK cells

NAD$^+$/NADH extraction buffer (S0175; Beyotime) was gently added. Following centrifugation at 12,000 g, 4°C for 10 min, the supernatant was collected as the test sample. For total NAD$^+$ and NADH measurement, 20 μL of the test sample was transferred to a 96-well plate. NADH was specifically measured by heating the samples at 60°C for 30 min to decompose NAD$^+$. A 96-well plate was then prepared incorporating blank controls and sample wells. A 20-μL test sample and a 90-μL ethanol dehydrogenase working solution were then added. After a 10-min incubation at 37°C in the dark to facilitate the conversion of NAD$^+$ to NADH, a 10-μL chromogenic reagent was added and the mixture was further incubated at 37°C in the dark for 30 min until an orange-yellow formazan developed. The concentration of NAD$^+$:NADH in the samples was calculated.

Statistical analysis

The statistical analysis and plotting were performed using R software (4.1.0). The difference between the two groups was evaluated using Student's t-test. The correlation between two continuous variables was determined by Spearman's correlation coefficient. The *mean ± SD* was presented for all values. All *P*-values were two-sided, and statistical significance was set at a $P < 0.05$.

Results

Activation of NK cytotoxic pathways in BRCA patients with elevated *LDHB* expression

To determine the potential role of *LDHB* in BRCA, we divided BRCA patients from TCGA into two groups based on high and low levels of *LDHB* expression. Subsequently, a comprehensive analysis was performed to identify DEGs between these two groups (**Figure 1A**). Notably, GSEA revealed a significant upregulation of the NK cell-mediated cytotoxicity pathway in the high *LDHB* group (**Figure 1B**). Additionally, we noted a significant pathway upregulation known for vital contributions to immunity and inflammation in the high *LDHB* group. Specifically, the chemokine signaling, the NF-κB signaling, and the cytokine-cytokine receptor interaction pathways demonstrated notable increases in activity (**Figure 1B, C**). The GO analysis consistently yielded similar results (**Figure S1A**). Moreover, the second- (graft-versus-host disease) and third-ranked pathways (rheumatoid arthritis) were

disease-associated with well-established links to NK cells[39,40] (**Figure 1B**). To further assess the effect of *LDHB* on NK cell-killing function, a comparative genetic analysis was performed between patients with high and low *LDHB* expression. The analysis revealed a significant upregulation of genes associated with NK cell cytotoxicity in the high *LDHB* expression group (**Figure 1D**). In addition, the genes involved in NK cell-killing functions, such as *GZMB*, *IFNG*, *ULBP3*, *FNAR2*, *TNF*, and *ULBP1*, were highly expressed in the high *LDHB* group of patients with BRCA (**Figure S1B-G**). These findings collectively support the hypothesis that BRCA patients with high *LDHB* expression exhibit an inflammatory phenotype and activate NK cytotoxic pathways.

Ldhb inhibits BRCA metastasis *in vitro* and *in vivo*

To determine how *Ldhb* activates NK cell-killing function in our model, we initially assessed the impact of *Ldhb* on the functional properties of BRCA cells. In our study, we initially observed a notable reduction in *LDHB* expression among patients with BRCA (**Figure 2A, B**), which emphasized the potential role of *LDHB* expression in BRCA pathogenesis. We established the stable cell lines, 4T1-*Ldhb* and BT-549-*LDHB*, which express *LDHB* in murine and human BRCA cells, respectively. Additionally, a control group was generated using a vector construct (**Figures 2C and S2A**). We systematically examined phenotypic characteristics *in vitro*. Specifically, our results showed that *Ldhb* suppresses the migration and invasion of BRCA cells (**Figure 2E, F**) without affecting proliferation and viability (**Figures 2D and S2B, C**). Furthermore, we demonstrated the inhibitory effect of *LDHB* on 4T1 pulmonary metastasis *in vivo* using a murine model (**Figure 2G-K**). In summary, these findings indicated that *Ldhb* does not affect the proliferation of 4T1 cells. However, *Ldhb* also has a crucial role in suppressing tumor cell migration and invasion.

Ldhb promotes the tumor reverse Warburg effect and reduces lactic acid secretion

As a crucial subunit of lactate dehydrogenase (LDH) at the end of glycolysis, LDHB has a pivotal role in metabolism. To comprehensively show the influence of *Ldhb* on metabolic pathways, we performed metabolomic profiling of 4T1-Vector and 4T1-*Ldhb* cells. The partial least squares (PLS) plot demonstrated distinct metabolic clustering patterns, highlighting the

disparities between the two cell populations (**Figure 3A**). We carefully illustrated the disparities among the top 25 metabolites in 4T1-*Ldhb* and 4T1-Vector cells with a heatmap representation, effectively accentuating the profound impact of *Ldhb* on tumor cell metabolism (**Figure 3B**). We determined that *Ldhb* orchestrated the multifaceted modulation of metabolic pathways within BRCA cells through an exhaustive analysis of differential metabolites. Specifically, *Ldhb* exerted a stimulating influence on pivotal pathways, such as sphingolipid metabolism, glutathione metabolism, and the citrate

cycle (**Figure 3C**), concomitantly downregulating the tyrosine metabolism pathway as well as porphyrin and chlorophyll metabolism (**Figure S3A**). Notably, the influence of *Ldhb* on sphingolipid metabolism suggests that *Ldhb* has a role in regulating cell membrane composition. Furthermore, in agreement with previous observations emphasizing the dominant Warburg effect in tumor cells, a phenomenon typically associated with citrate cycle inhibition, our findings elucidated the active role of *Ldhb* in promoting the citrate cycle, resulting in the augmentation of metabolites within the citric acid pathway
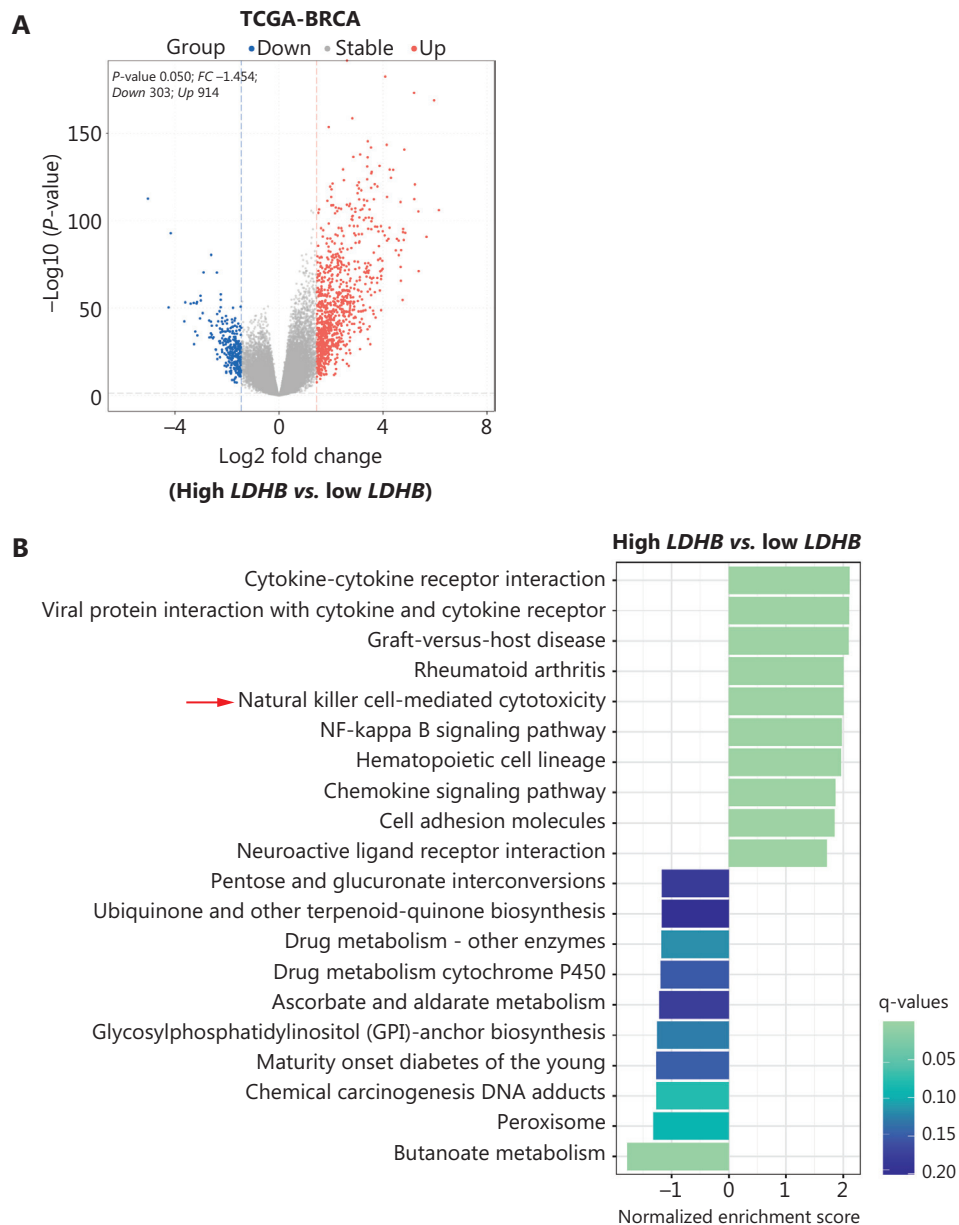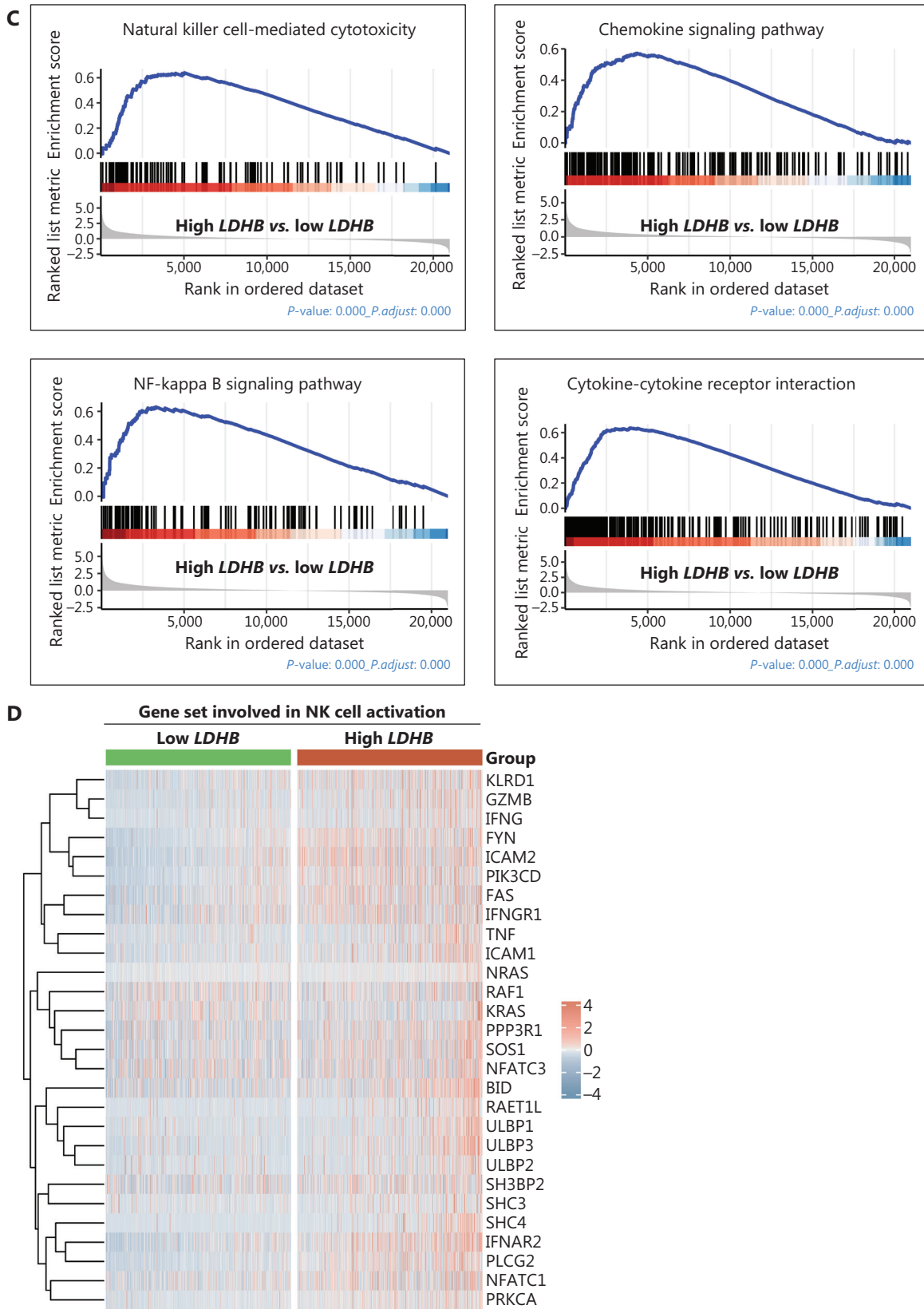

Figure 1 Continued

C

Natural killer cell-mediated cytotoxicity

Chemokine signaling pathway

High *LDHB* vs. low *LDHB*

High *LDHB* vs. low *LDHB*

P-value: 0.000_P.adjust: 0.000

P-value: 0.000_P.adjust: 0.000

NF-kappa B signaling pathway

Cytokine-cytokine receptor interaction

High *LDHB* vs. low *LDHB*

High *LDHB* vs. low *LDHB*

P-value: 0.000_P.adjust: 0.000

P-value: 0.000_P.adjust: 0.000

D Gene set involved in NK cell activation

Low *LDHB*   High *LDHB*   Group

KLRD1
GZMB
IFNG
FYN
ICAM2
PIK3CD
FAS
IFNGR1
TNF
ICAM1
NRAS
RAF1
KRAS
PPP3R1
SOS1
NFATC3
BID
RAET1L
ULBP1
ULBP3
ULBP2
SH3BP2
SHC3
SHC4
IFNAR2
PLCG2
NFATC1
PRKCA

Figure 1 Continued

Figure 1 Activation of NK cytotoxic pathways in breast cancer patients with elevated *LDHB* expression. (A) Volcano plot displaying the differential gene expression between the *LDHB* low and high groups from the TCGA-BRCA dataset. The x-axis represents the log2 fold-change and the y-axis represents the negative log10 *P*-value. The red dots indicate upregulated genes, while the blue dots indicate downregulated genes. (B) Gene Set Enrichment Analysis (GSEA) was performed to identify differentially enriched pathways between the *LDHB* low and high group. The Kyoto Encyclopedia of Genes and Genomes (KEGG) database was used for pathway annotation. The top enriched pathways were shown in the bar plots with the normalized enrichment score (NES) and q-values indicated. (C) Upregulated GSEA signatures in *LDHB*-high group are depicted using data from TCGA-BRCA dataset (*P* < 0.001). Four representative pathway diagrams were displayed. (D) Heatmap of gene expression profiles related to NK cell cytotoxicity in two groups with differential *LDHB* expression. Each row represents a gene and each column represents an individual sample. Gene expression is color-coded according to the key on the right. The *LDHB*-high group is indicated in red and the *LDHB*-low group is indicated in green.

(**Figures 3D, E and S3B**). Consequently, *Ldhb* promoted a shift in BRCA cells towards the reverse Warburg effect. Moreover, we examined several important metabolic indices and observed that *Ldhb* overexpression further reduced lactic acid secretion and enhanced glucose uptake by tumor cells (**Figures 3F, G and S3C**). Notably, the NAD$^+$:NADH ratio, which reflects intracellular metabolism and redox status, was significantly reduced in tumor cells overexpressing *Ldhb* (**Figure 3H**), which may be responsible for a significant increase in reactive oxygen species (ROS) levels (**Figure 3I**).

Monocarboxylate transporter 1 (MCT1) and monocarboxylate transporter 4 (MCT4) are important carriers of cells[41,42]. Analysis of BRCA in TCGA and the Cancer Cell Line Encyclopedia (CCLE) confirmed that *MCT1* but not *MCT4* had a strong positive correlation with *LDHB* (**Figure 3J, K**). In addition, real-time PCR indicated significant upregulation of *Mct1* expression in 4T1-*Ldhb* and BT-549-*LDHB* cell lines (**Figure 3L, M**), which supported the proposition that LDHB has a dual role in lactic acid clearance. Functioning as a molecular sponge, *LDHB* efficiently eradicates lactic acid by facilitating the intracellular conversion to pyruvate. Concurrently, *LDHB* orchestrates the upregulation of *MCT1*, thereby amplifying extracellular lactic acid uptake. In summary, *LDHB* drives the reverse Warburg effect in BRCA cells, culminating in a reduction in lactic acid levels within the TME.

Ldhb drives NK cell activation through lactic acid reduction in the TME

Next, we determined whether and how *LDHB* in BRCA cells affects the activity of NK cells. *LDHA* and *LDHB* are the key LDH subunits that regulate the conversion of pyruvate to lactic acid[43]. *LDHB* is also thought to be a scavenger of intracellular lactic acid[28], while previous studies have defined the critical contribution of lactic acid as an effector metabolite associated with the inactivation of NK and T cells[23]. Based on previous studies and our findings, we hypothesized that *LDHB* may have a regulatory role in mitigating lactic acid secretion, ultimately potentiating the cytotoxic efficacy of NK cells. To test this hypothesis, we isolated primary NK cells from the spleens of BALB/c mice using flow cytometry (**Figure 4A**). Subsequently, the cells were exposed to a conditioned medium derived from the 4T1-Vector and 4T1-*Ldhb* cells, which were untreated, pretreated with 10 mM sodium oxamate, or supplemented with 10 mM lactic acid. The lactic acid levels in 4T1-*Ldhb* and BT-549-*LDHB* CM were reduced and sodium oxamate effectively suppressed lactic acid secretion (**Figure 4B, C**). Treating NK cells with 4T1-*Ldhb* CM promoted cell viability, which was counteracted by the exogenous addition of lactic acid. Conversely, inhibition of lactic acid secretion by sodium oxamate enhanced these effects (**Figure 4D**). Furthermore, after exposure to 4T1-*Ldhb* CM, NK cells demonstrated increased expression of IFN-γ and an augmented cytotoxic potential. Notably, this enhancement was significantly inhibited by lactic acid addition (**Figure 4E**). Next, we co-cultured NK cells with 4T1 cells and exposed the combined cells to 4T1-Vector CM or 4T1-*Ldhb* CM to assess NK cell cytotoxicity against BRCA cells. Notably, 4T1-*Ldhb* CM significantly potentiated the cytotoxicity of NK cells against 4T1 tumor cells. This enhanced cytotoxic effect was effectively attenuated by the addition of exogenous lactic acid (**Figure 4F**). These findings confirmed the pivotal role of lactic acid in 4T1-*Ldhb* CM by modulating the effector functions of NK cells. Our results underscore the pivotal role of BRCA cell *LDHB* in modulating NK cell activity through lactic acid

10

Luo et al. Diminished *LDHB* in breast tumors impedes NK cells

regulation, emphasizing the significance of *LDHB* in regulating NK cell-mediated anti-tumor responses.

High expression of *Ldhb* activates NK cells and suppresses tumor growth *in vivo*

Further, we established a subcutaneous tumorigenesis model in BALB/c mice to investigate the *in vivo* impact of *Ldhb* to functionally confirm the significance of *Ldhb* in BRCA for NK cell-mediated cytotoxicity. We administered 4T1-Vector and 4T1-*Ldhb* cells into the subcutaneous tissues of BALB/c mice.

The results obtained from the *in vivo* experiments differed from the results of *in vitro* experiments. Notably, we observed a substantial reduction in tumor size in the 4T1-*Ldhb* group (**Figure 5A**-C). To determine whether lymphocytes and/or NK cells in the TME contribute to tumor growth inhibition, we injected 4T1-*Ldhb* and control cells into immunodeficient NOD-SCID mice (*Prkdc$^{-/-}$* lacking T and B cells) and NSG mice (*Prkdc$^{-/-}$* IL2rg$^{-/-}$ lacking T, B, and NK cells). Tumors in the 4T1-*Ldhb* group of NOD-SCID mice were consistently reduced in size compared to the control group (**Figure 5D-F**). However, no significant difference in tumor size was
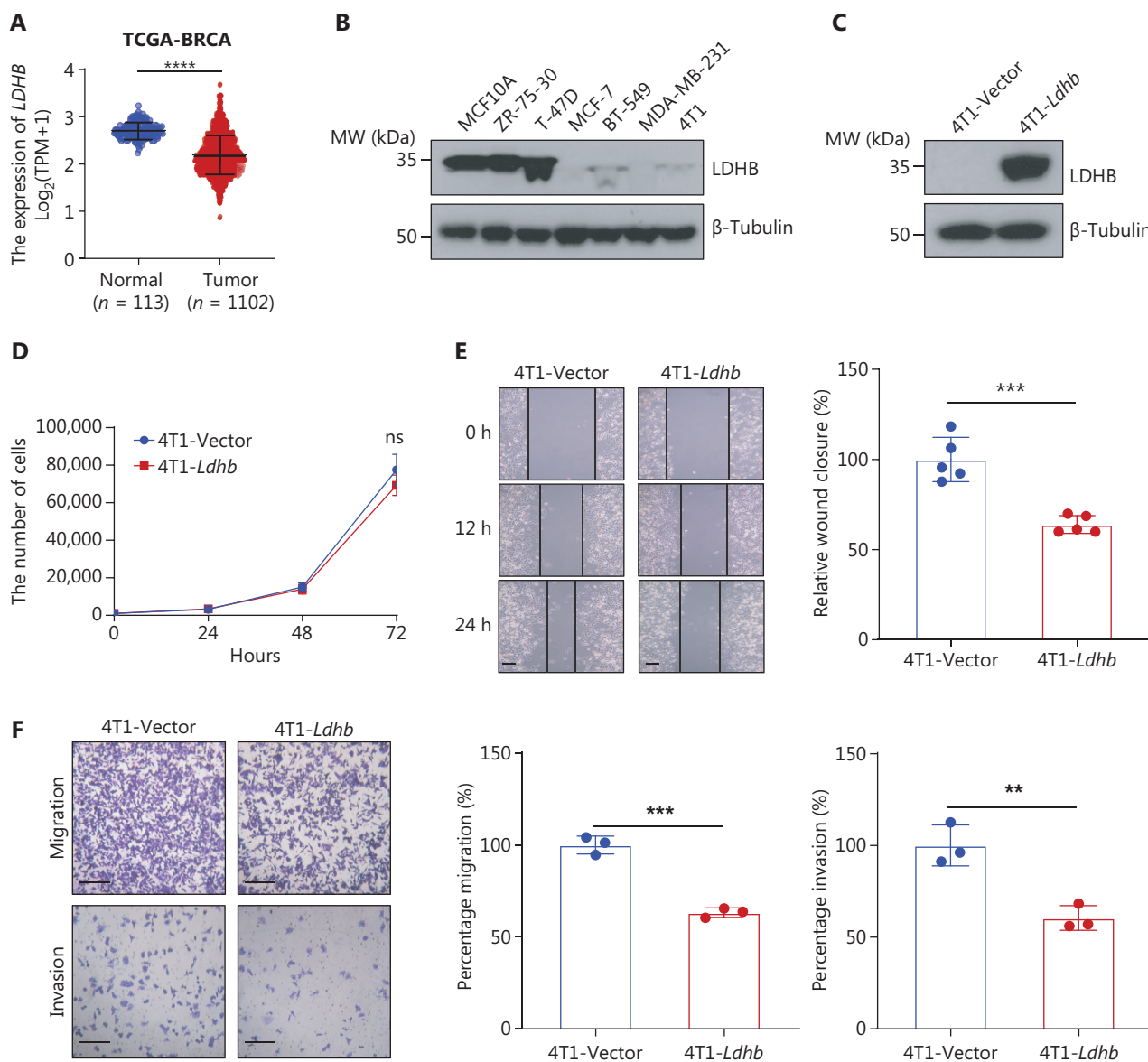
Figure 2 Continued
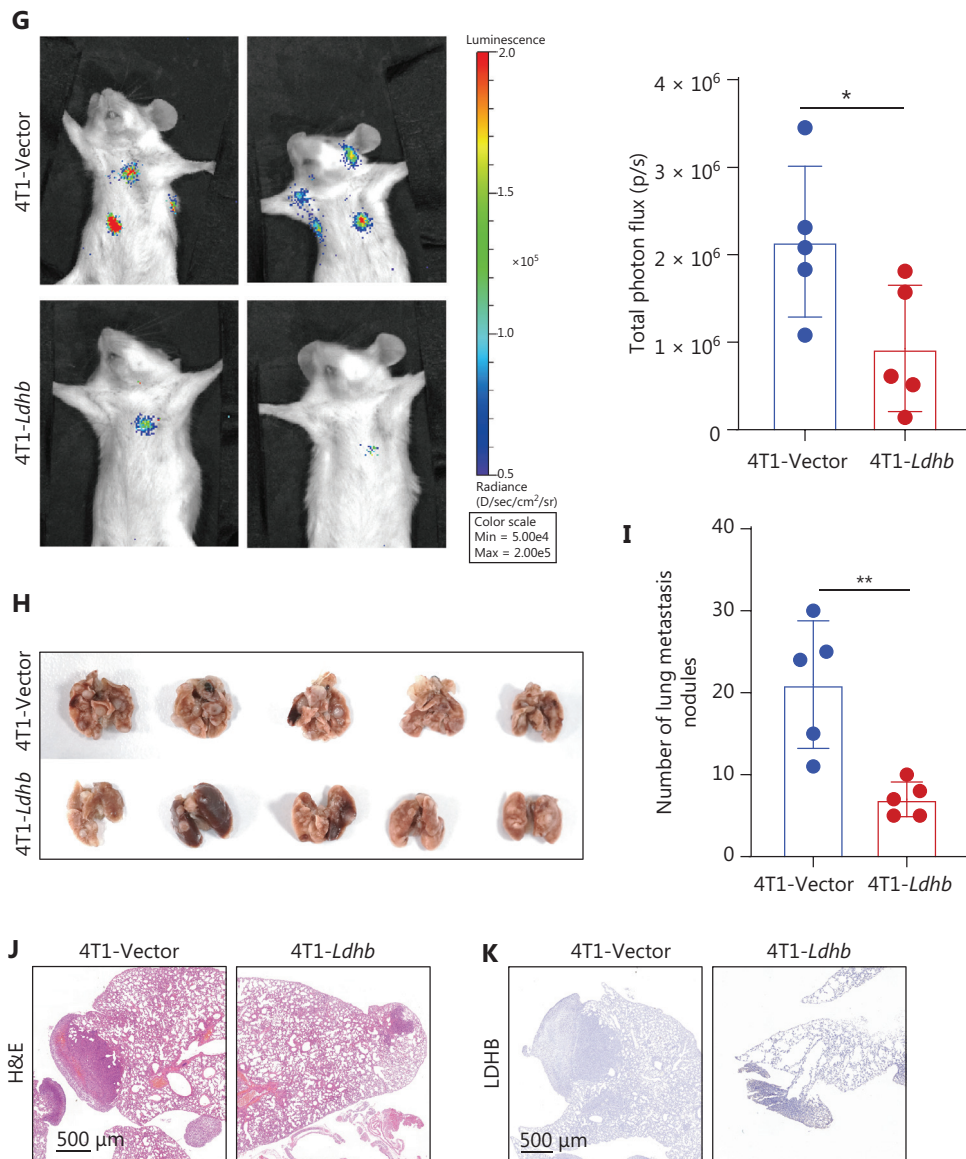
Figure 2   *Ldhb* inhibits breast tumor metastasis *in vitro* and *in vivo*. (A) Graph depicting the levels of *LDHB* expression in healthy and breast cancer patients. The data were obtained from the TCGA breast cancer dataset. (B) Western blot analysis of *LDHB* protein expression in six breast cancer cell lines (ZR-75-30, T-47D, MCF-7, BT-549, MDA-MB-231, and 4T1) and a normal breast cell line (MCF10A). β-Tubulin was used as the loading control. MW (kDa) represents the molecular weight in kilodaltons. (C) Western blot analysis of Ldhb in 4T1 cells transfected with empty vector (4T1-Vector) and cells transfected with *Ldhb* (4T1-*Ldhb*). β-Tubulin was used as a loading control. (D) The proliferation of 4T1-Vector and 4T1-*Ldhb* cells was determined by counting the number of cells. (E) Scratch assays of 4T1-Vector and 4T1-*Ldhb* cells and the photomicrographs showing scratches at 0, 12, and 24. Representative images are shown and the migrated cells were counted. Scale bars = 200 μm. Statistical data are shown. (F) The migration and invasion abilities of 4T1-Vector and 4T1-*Ldhb* cells were detected by Transwell assays. Scale bar = 200 μm. (G) Representative images of *in vivo* imaging in a murine lung metastasis model. 10^5 4T1-*Ldhb* or control cells were intravenously injected into the tail vein, followed by the injection of potassium luciferin for bioluminescence imaging 4 weeks later. The right panel depicts the statistical analysis of total photon flux (p/s) for each mouse. *n* = 5 mice per group. (H) Lung images derived from mice in the lung metastasis model. (I) The bar graph illustrates quantification of lung metastasis nodules of each mouse. (J) Hematoxylin and eosin (HE) staining images depict the metastatic status of 4T1-*Ldhb* or control cells. Scale bar = 500 μm. (K) Immunohistochemical (IHC) staining of LDHB protein in the lungs of mice after tail vein injection of 4T1-*Ldhb* or control. Scale bar = 500 μm. In all the analyses, the results represent the *mean ± SD*. *P*-values were calculated using a two-tailed unpaired t-test. *P* < 0.05 was considered significant (**P* < 0.05, ***P* < 0.01, ****P* < 0.001, *****P* < 0.0001; "ns" indicates non-significance).

observed between the 4T1-*Ldhb* and control groups in NSG mice (**Figure 5G-I**). These findings highlight the functional involvement of NK cells in *Ldhb*-induced inhibition of tumor growth. Next, we used flow cytometry to evaluate immune cell populations in tumor tissues. We observed no significant changes in the number of CD4$^+$ T cells, CD8$^+$ T cells, or NK cells between the 4T1-*Ldhb* and control (**Figures 5J, K and S4A, B**). Our previous bioinformatic analysis identified the activation of NK cell-mediated cytotoxicity in the *LDHB*-high

group. In agreement with our previous findings, flow cytometry and immunofluorescence analyses revealed an elevation in IFN-γ and granzyme B at the protein level within NK cells, which confirmed the increased activation of NK cell-mediated cytotoxicity in the 4T1-*Ldhb* group (**Figures 5L, M and S4C, D**). Moreover, real-time quantitative PCR revealed upregulation of genes related to NK cell activation, such as *Infg* and *Gzmb*, in the 4T1-*Ldhb* group (**Figure S4E, F**). Furthermore, we observed a significant reduction in lactic acid levels in the
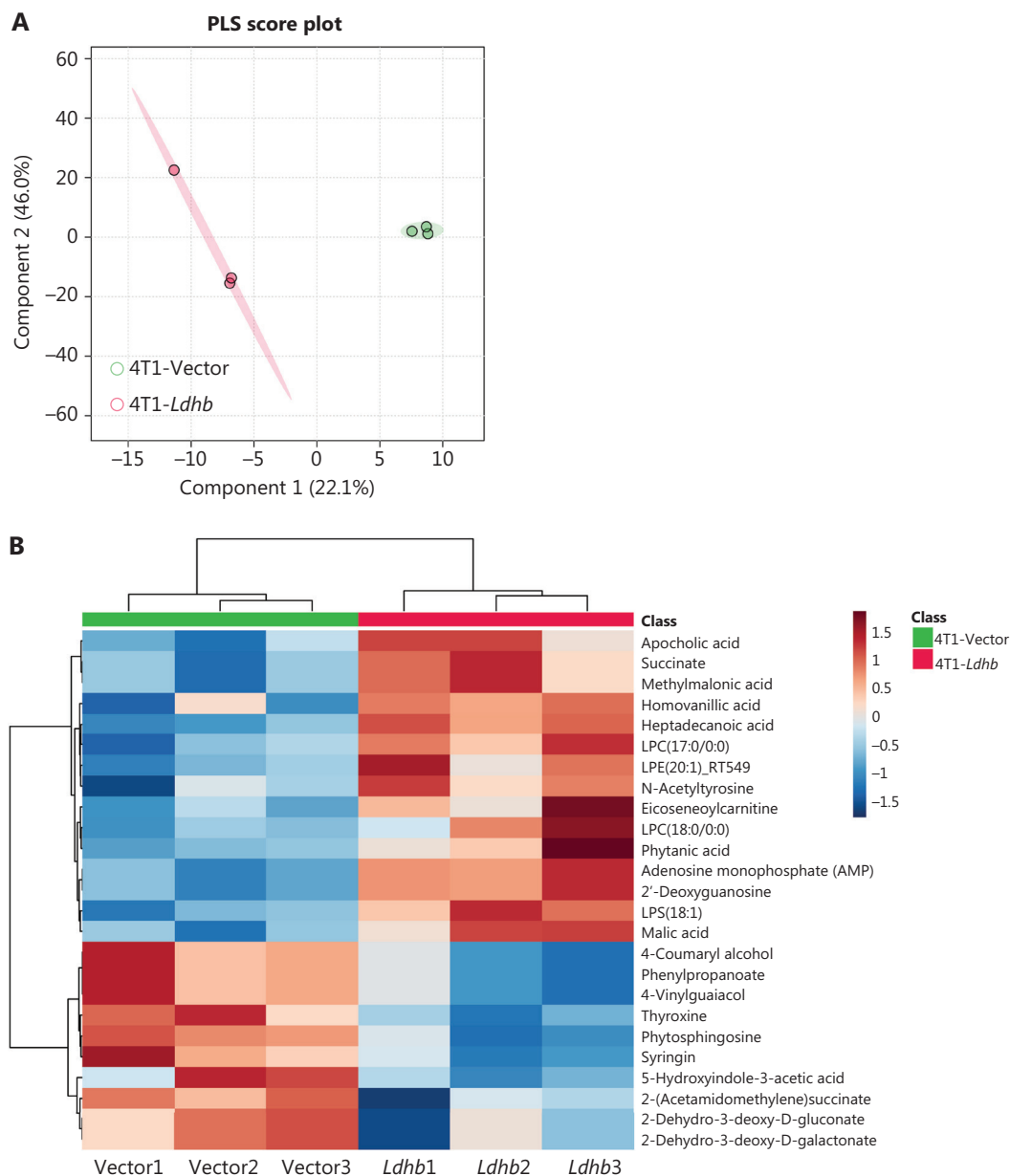
Figure 3 Continued

4T1-*Ldhb* group (**Figure S4G**), accompanied by an increase in the expression of the lactic acid transporter receptor, *Mct1* (**Figure S4H**), which is consistent with our *in vitro* cell experiments. Collectively, these data support a model in which *Ldhb* overexpression in tumor cells enhances NK cell-mediated cytotoxicity and inhibits tumor progression.

Enhanced *LDHB* expression in BRCA patients is correlated with NK cell activation

To verify the ability of *LDHB* to promote NK cell activation in clinical samples, we performed transcriptome sequencing of nine patients with BRCA. We grouped patients according to
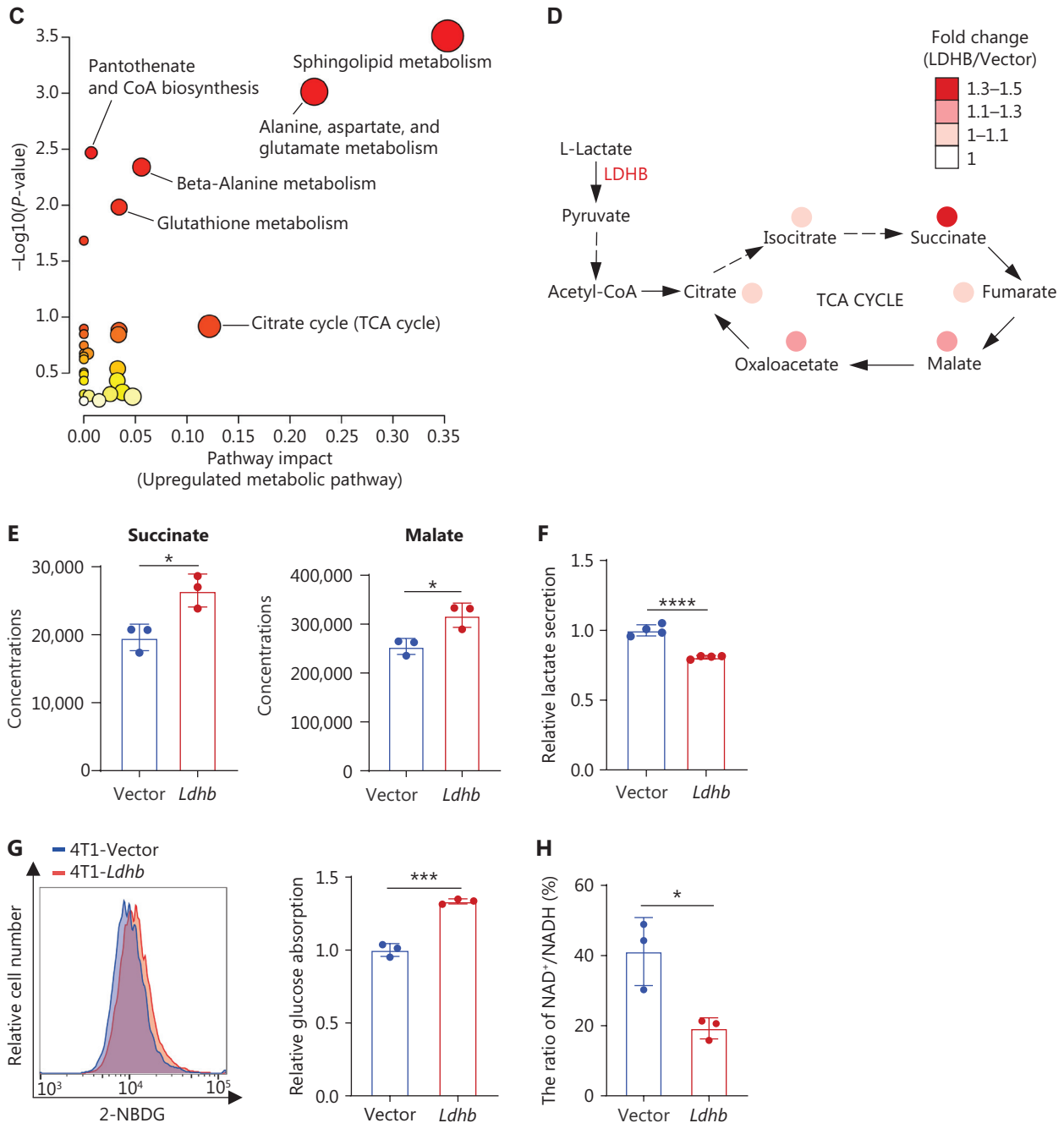
Figure 3   Continued
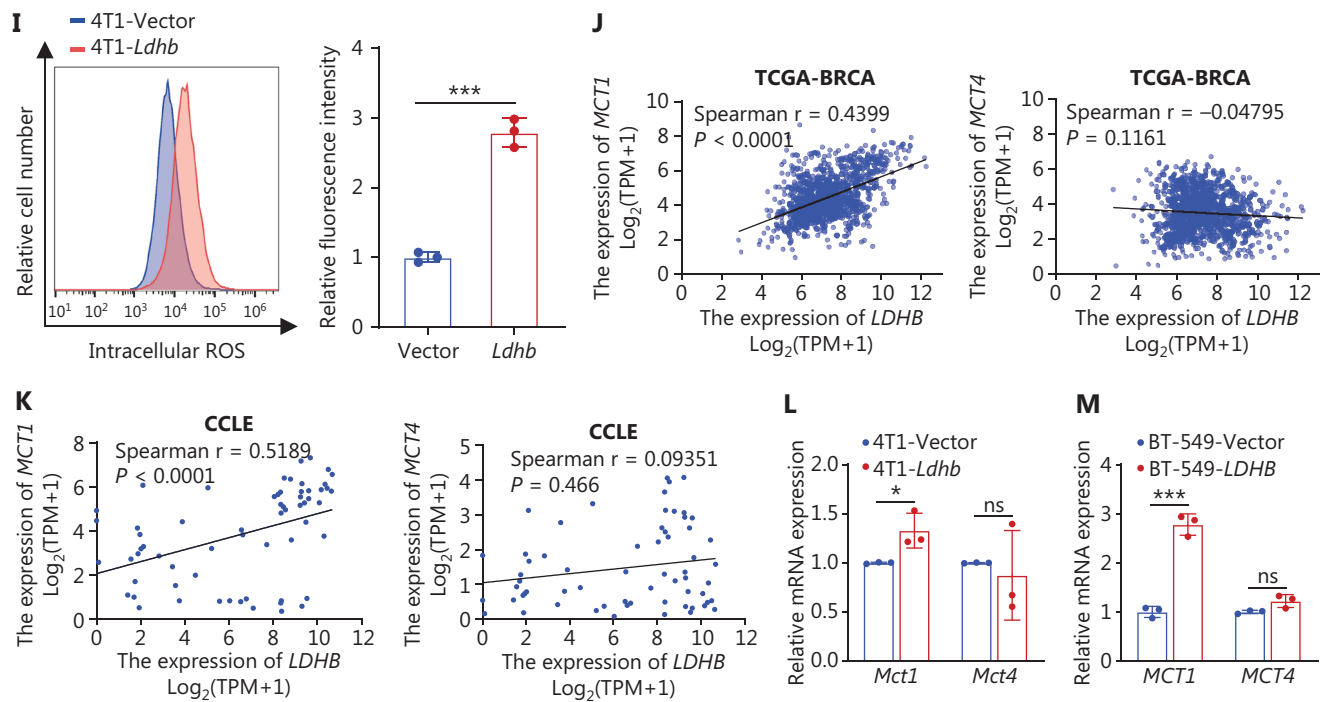
Figure 3 *Ldhb* promotes the tumor reverse Warburg effect and reduces lactic acid secretion. (A) Partial least squares (PLS) analysis comparing the metabolomic profiles of the 4T1-Vector (*n* = 3) and 4T1-*Ldhb* group (*n* = 3) samples. Each point represents an individual sample. (B) Heatmap representation of the top 25 differential metabolites between 4T1-*Ldhb* and 4T1-Vector cells. Color intensity reflects relative metabolite abundance. (C) Enrichment analysis of upregulated metabolic pathways for 4T1-*Ldhb* cells using KEGG pathway enrichment. The size and color of the dots indicate the enrichment level and significance, respectively. (D) Illustration of specific metabolites within the tricarboxylic acid (TCA) cycle. The depicted abundance is presented as the ratio of metabolite levels in the 4T1-*Ldhb* and 4T1-Vector groups, with color intensity indicating the magnitude of change. Deeper colors signify higher fold-changes. (E) Metabolite levels of succinate and malate in 4T1-Vector and 4T1-*Ldhb* cells. (F) Concentration of lactate in conditioned medium (CM) from 4T1-Vector and 4T1-*Ldhb* cells. (G) Glucose uptake capacity of 4T1-Vector and 4T1-*Ldhb* cells monitored by 2-NBDG fluorescence. After 1 h of starvation, cells were exposed to 5 µM 2-NBDG for 30 min and analyzed by flow cytometry. (H) Intracellular NAD^+:NADH ratios of 4T1-Vector and 4T1-*LDHB* cells. (I) ROS levels of 4T1-Vector and 4T1-*Ldhb* cells were detected by flow cytometry with a 10 µM carboxylated H2DCFDA analog [carboxy-H2DCFDA (C400)]. (J-K) Correlation between *LDHB* and *MCT1* or *MCT4* expression from TCGA-BRCA (J) and CCLE data (K). Spearman coefficient was used to assess significance and a line of best fit is shown (black line). (L) qRT-PCR analysis of *Mct1* and *Mct4* mRNA in 4T1-Vector and 4T1-*Ldhb* cells. Results are normalized to *Gapdh* mRNA and presented as relative expression compared with 4T1-Vector cells. (M) qRT-PCR analysis of *MCT1* and *MCT4* mRNA in BT-549-Vector and BT-549-*LDHB* cells. Results are normalized to *GAPDH* mRNA and presented as relative expression compared with BT-549-Vector cells. In all the analyses, the results represent the *mean ± SD*. *P*-values were calculated using a two-tailed unpaired t-test. *P* < 0.05 was considered significant (*P < 0.05, ***P < 0.001, ****P < 0.0001; "ns" indicates non-significance).

LDHB expression based on the sequencing results (**Figure 6A**). Patients with elevated *LDHB* expression had a corresponding marked increase in the level of NK cell activity marker (*GZMB* and *IFNG*) expression (**Figure 6B, C**). Moreover, ssGSEA further confirmed the pronounced activation of NK cells (**Figure 6D**). Immunofluorescence analysis of the tissue revealed a pronounced elevation in CD16 expression, an activating receptor in NK cells, along with an increased granzyme B protein level in patients with high *LDHB* expression (**Figures 6E and S5A**). To gain further insight into the immune

cell landscape within the TME, we analyzed single-cell RNA sequencing (scRNA-seq) data from five breast cancer tissues. A uniform manifold approximation and projection (UMAP) clustering plot and heatmap were used to identify distinct cell populations based on known cell type-specific markers (**Figure 6F, G**). Primary BRCA patients were stratified into two groups based on the expression of *LDHB* in tumor cells (**Figures 6H and S5B**). Our data revealed a significant increase in T and NK cell infiltration in the high *LDHB* group compared to the low *LDHB* group (**Figure 6I**). Additionally, analysis of

the single-cell map indicated a significantly higher frequency of IFNG+ NK cells in the high *LDHB* group (**Figures 6J and S5C, D**), implying a potential role of *LDHB* in modulating immune responses in BRCA. In summary, these results further validated that BRCA patients with high *LDHB* expression promoted NK cell activation, potentially boosting anti-tumor immune function.

LDHB facilitates the formation of a tumor immune-enhancing microenvironment in TCGA

Immune cells are an essential part of the TME and have an important role in tumor development and inhibition. To further investigate if *LDHB* affects immune cells in the TME, we
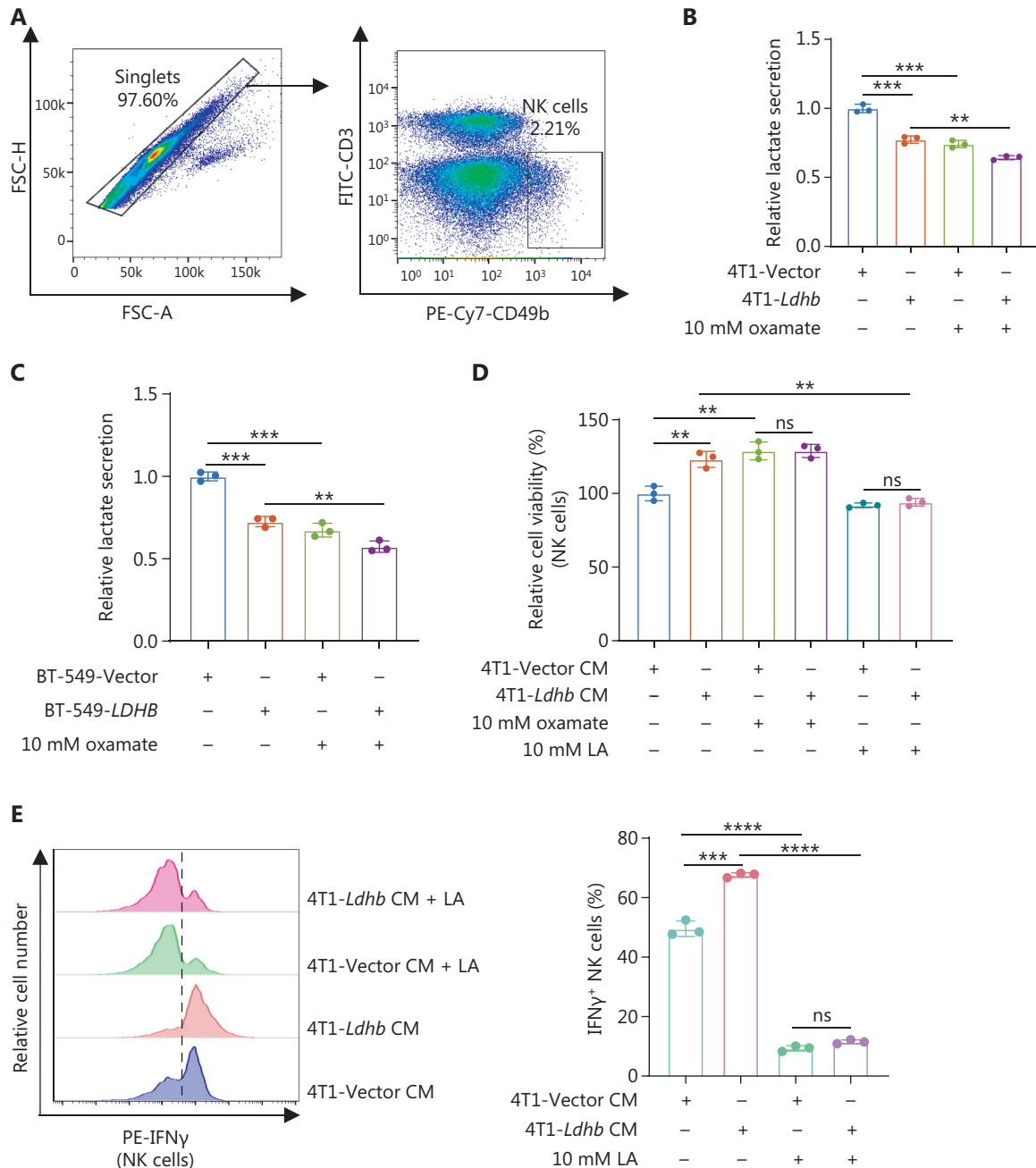
Figure 4 Continued
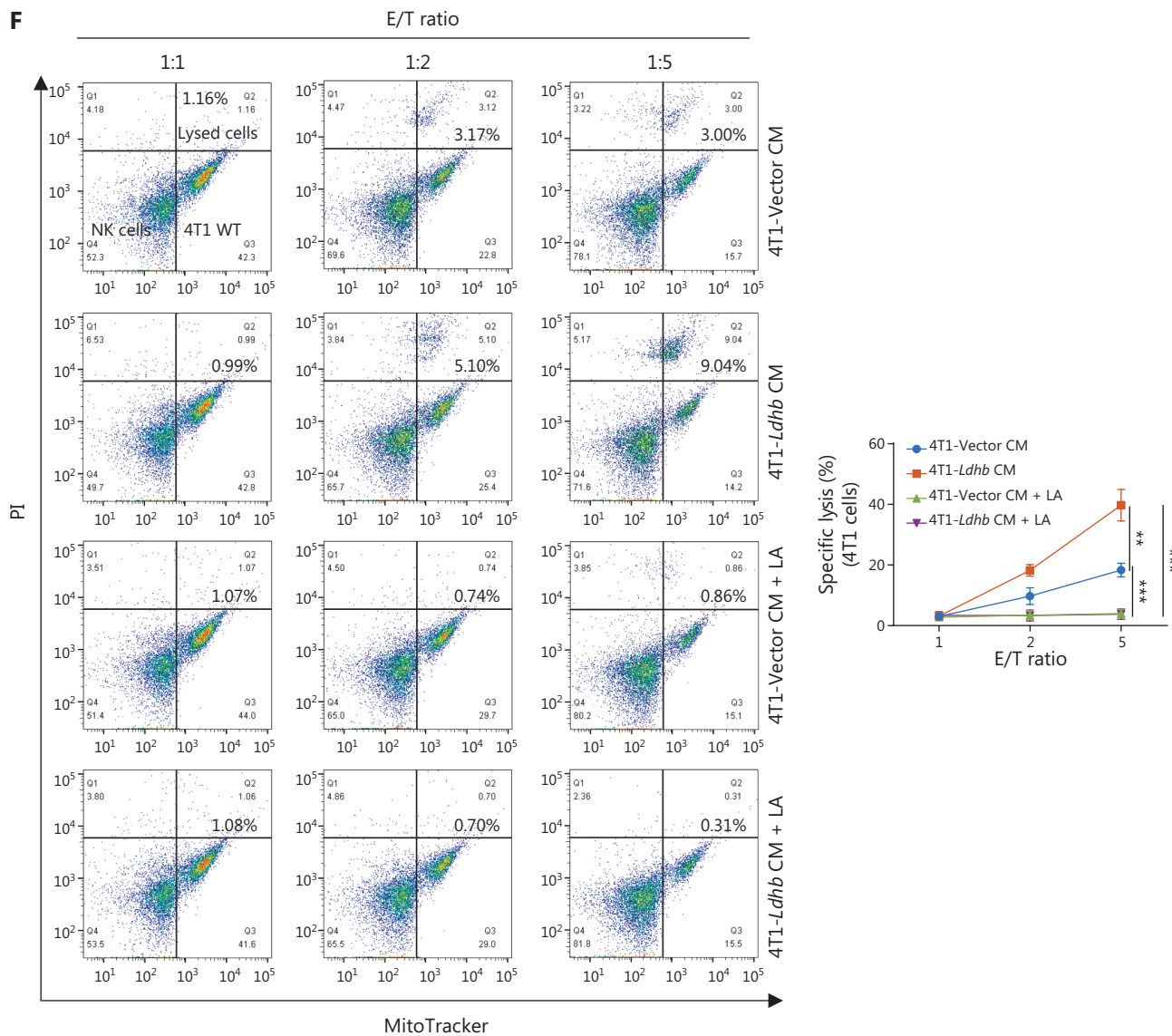
Figure 4 *Ldhb* drives NK cell activation through lactic acid reduction in the tumor microenvironment. (A) Flow cytometry gating strategies were employed to isolate NK cells (defined as CD3⁻CD49b⁺) from the spleens of BALB/c mice. (B) Lactate secretion capacity in 4T1-Vector and 4T1-*Ldhb* cells under untreated and 10 mM sodium oxamate-treated conditions. (C) Lactate secretion capacity in BT-549-Vector and BT-549-*LDHB* cells under untreated and 10 mM sodium oxamate-treated conditions. (D) NK cell viability was assessed under various culture conditions. NK cells were cultured for 5 days in different culture media and viability was determined using the CCK-8 assay. The culture media were derived from the supernatants collected from 4T1-Vector and 4T1-*Ldhb* cells, either untreated or pre-treated with 10 mM sodium oxamate, or supplemented with 10 mM lactic acid. (E) Flow cytometric analysis of IFNγ⁺ cells among stimulated NK cells after incubation with the conditioned medium from 4T1-Vector (4T1-Vector CM) or 4T1-*Ldhb* cells (4T1-*Ldhb* CM) in the absence or presence of lactic acid (LA) for 24 h. One representative experiment of three is shown (left panel). The percentage of IFNγ⁺ NK cells was counted after treatment (right panel). *n* = 3 independent experiments. (F) NK cytotoxic assay. NK cells from the spleen of BALB/c mice were incubated with 4T1 target cells for 4 h at 37°C and in the presence of rIL-2 (1,000 U/mL). Each effector-to-target (E: T) ratio was analyzed by flow cytometry. The representative flow cytometry results are presented on the left with the corresponding apoptosis statistics for 4T1 target cells post-PI staining depicted on the right. Each experimental set was independently replicated three times. In all the analyses, the results are expressed as the *mean* ± *SD*. *P*-values were calculated using a two-tailed unpaired t-test. *P* < 0.05 was considered significant (**P < 0.01, ***P < 0.001, ****P < 0.0001; "ns" indicates non-significance).

conducted a comprehensive analysis of a cohort of 1,072 patients with BRCA obtained from TCGA. By integrating clinical prognostic information with immune cell infiltration data, we derived patient survival profiles that reflected the anti-tumor functionality of immune cells (**Figure S6A**). The majority of immune cells responsible for tumor suppression, such as T cells and M1 macrophages, exhibited increased levels of infiltration in patients with high *LDHB* expression. Conversely, immune cells associated with tumor promotion, such as Tregs and M2 macrophages, were downregulated (**Figure 7A**). These findings indicate a shift in the immune cell landscape towards enhanced anti-tumor immunity in patients with high *LDHB* expression. Moreover, correlation analysis revealed a robust association between distinct immune cell populations within the high *LDHB* group (**Figure S6B**), suggesting an increased interplay between diverse

immune cells in patients with high *LDHB* expression. Our data showed that NK cells exhibit distinct functionalities between the two groups. In the low *LDHB* group, NK cell infiltration did not significantly affect the OS of patients (HR = 1.2231, *P* = 0.3827). However, upregulation of NK cell infiltration significantly prolonged patient survival in the high *LDHB* group (HR = 0.5942, *P* = 0.0235; **Figure 7B, C**), indicating that NK cells may kill tumors and prolong the lives of patients. Furthermore, Kaplan–Meier survival curves indicated that patients with elevated *LDHB* expression have enhanced activation of immune cells, including CD8^{+} T cells, conventional dendritic cells (cDCs), and Tregs, which together reflect increased immunologic function (**Figure 7D-I**). These results demonstrated that *LDHB* in BRCA modulates immune cell infiltration and function, thereby shaping a TME that promotes immunogenicity.
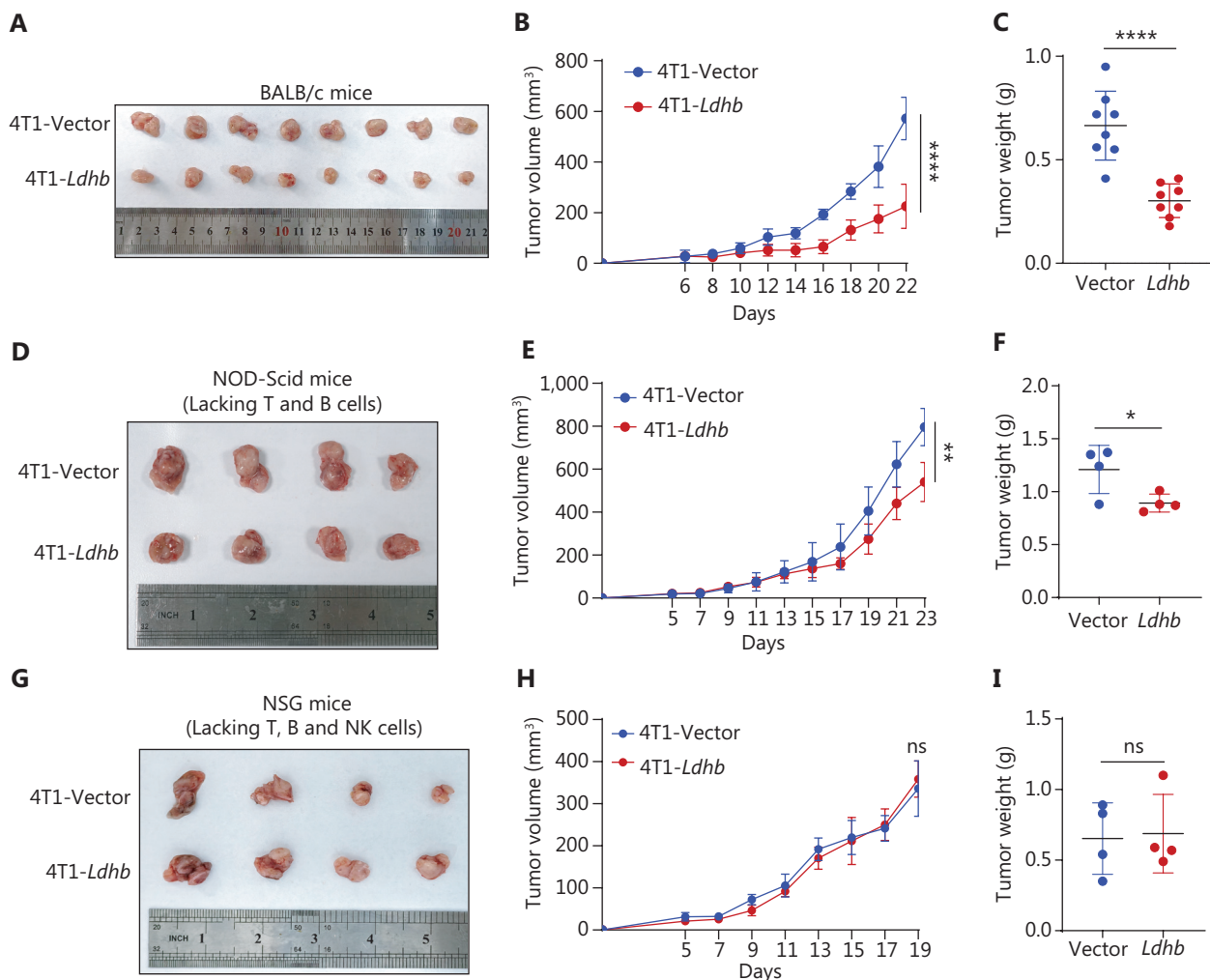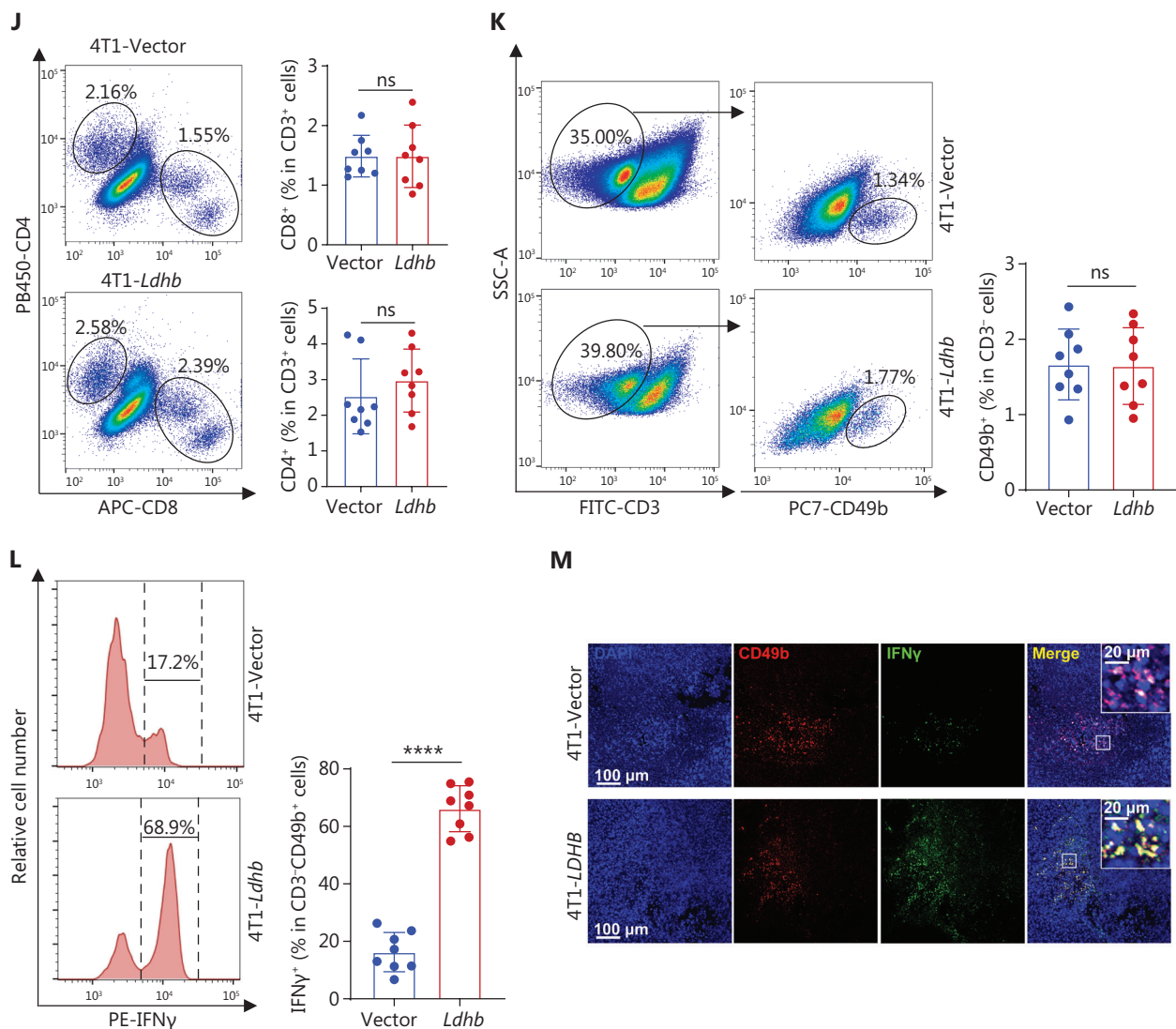

Figure 5   Continued

Figure 5 High expression of *Ldhb* activates NK cells and suppresses tumor growth *in vivo*. (A-C) Tumor growth in BALB/c mice was initiated by subcutaneous injection of 10^5 4T1-Vector and 4T1-*Ldhb* cells. Representative images illustrating tumor formation in each group are presented (A). The trajectory of tumor growth (B) and tumor weight (C) was monitored. n = 8 mice per group. (D-F) Tumor growth in immunodeficient NOD-SCID mice (Prkdc$^{-/-}$) was initiated by subcutaneous injection of 10^5 4T1-Vector and 4T1-*Ldhb* cells. Representative images illustrating tumor formation in each group are presented (D). The trajectory of tumor growth (E) and tumor weight (F) was monitored. n = 4 mice per group. (G-I) Tumor growth in immunodeficient NSG mice (Prkdc$^{-/-}$ IL2rg$^{-/-}$) was initiated by subcutaneous injection of 10^5 4T1-Vector and 4T1-*Ldhb* cells. Representative images illustrating tumor formation in each group are presented (G). The trajectory of tumor growth (H) and tumor weight (I) was monitored. n = 4 mice per group. (J) Gating strategy for flow cytometry analysis of CD4$^+$T cells (CD3$^+$CD4$^+$) and CD8$^+$T cells (CD3$^+$CD8a$^+$) in tumors from BALB/c mice after subcutaneous injection of 10^5 4T1-Vector or 4T1-*Ldhb* cells. The numbers in graphs indicate the percentage of cells. Plots of data from one representative immune cell type are shown. The proportion of CD4$^+$ and CD8$^+$ T cells among CD3$^+$ cells was quantified in BALB/c mouse tumors. Each symbol represents an individual mouse. n = 8 mice per group. (K) Gating strategy for flow cytometry analysis of NK cells (CD3$^-$CD49b$^+$) in tumors from BALB/c mice after subcutaneous injection of 10^5 4T1-Vector or 4T1-*Ldhb* cells. Numbers in graphs indicate the percentage of cells. Plots of data from one representative immune cell type are shown. The proportion of NK cells among CD3$^-$ cells was quantified in BALB/c mouse tumors. Each symbol represents an individual mouse. n = 8 mice per group. (L) Representative flow cytometric histogram plots and quantification of IFNγ$^+$ NK cells in tumors of BALB/c mice. (M) IFNγ immunofluorescence staining of the NK cells in tumors and CD49b was used as the marker. Scale bars = 100 μm (20 μm for the enlarged image). In all the analyses, results are expressed as the *mean ± SD*. *P*-values were calculated using a two-tailed unpaired t-test. *P* < 0.05 was considered significant (*P < 0.05, **P < 0.01, ****P < 0.0001; "ns" indicates non-significance).

Clinical correlations with *LDHB* and NK cell activation in tumors

Finally, to evaluate the clinical relevance of our findings, we analyzed *LDHB* expression in other tumors using publicly available TCGA data. We utilized a gene signature related to NK cell activation and performed ssGSEA to evaluate NK cell activation in each patient (**Figure 8A**). Patients with high *LDHB* expression had higher NK cell activation scores in BRCA, LIHC, and PAAD (**Figures 8B-D and S7A**). Furthermore, compared to LDHA, *LDHB* demonstrated superior precision in forecasting NK cell activation, with AUC values of 0.654,
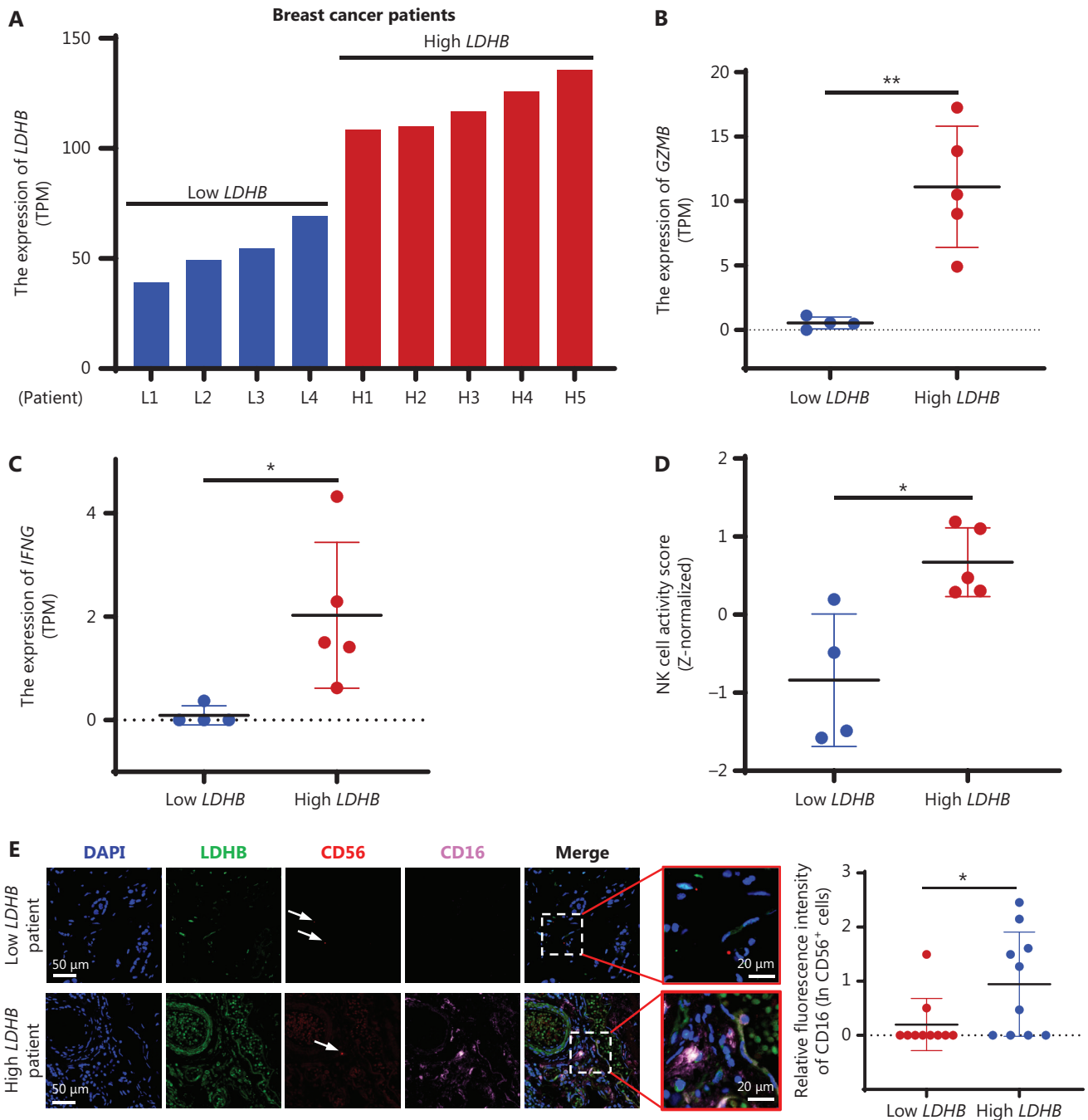
Figure 6   Continued
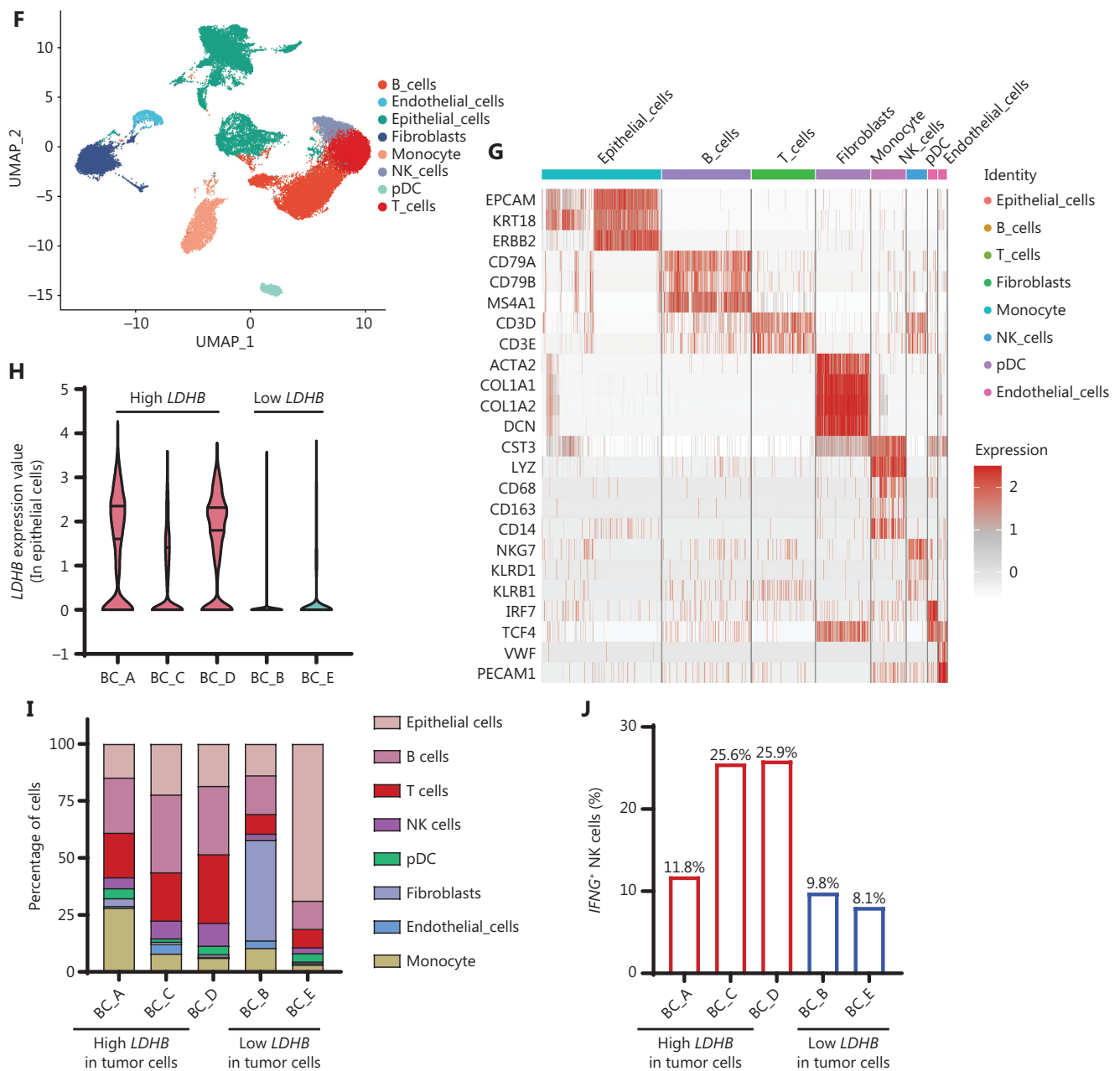
Figure 6 Enhanced *LDHB* expression in breast cancer patients correlates with NK cell activation. (A) The RNA sequencing results for 9 breast cancer patients display the gene expression levels of *LDHB* by transcripts per million (TPM). (B-C) The levels of *GZMB* (B) and *IFNG* expression (C) in patients with low and high expression of *LDHB*. (D) NK cell activity scores in patients with low and high LDHB expression were calculated using GSVA. (E) Representative tissue immunofluorescence images from patients with low (patient L1) and high LDHB (patient H5). CD56 labeling represents NK cells, while CD16 represents NK cell activity. Scale bars = 50 µm (20 µm for the enlarged image). The statistical graphs depict the results based on observations from 10 different perspectives. (F) Uniform manifold approximation and projection (UMAP) analysis of all cell types (*n* = 42,662) from scRNA-seq analysis of 5 primary breast cancer. (G) Heatmap illustrating the expression of established cell type-specific markers. Each column corresponds to an individual cell. (H) The violin diagram shows *LDHB* expression in tumor cells in 5 cases of primary breast cancer. (I) The stacked bars show the proportion of main cell type in 5 cases of primary breast cancer. (J) The proportion of IFNG+ NK cells derived from five breast cancer patients. In all the analyses, the results are expressed as the *mean ± SD*. *P*-values were calculated using a two-tailed unpaired t-test. *P* < 0.05 was considered significant (*P < 0.05, **P < 0.01; "ns" indicates non-significance).
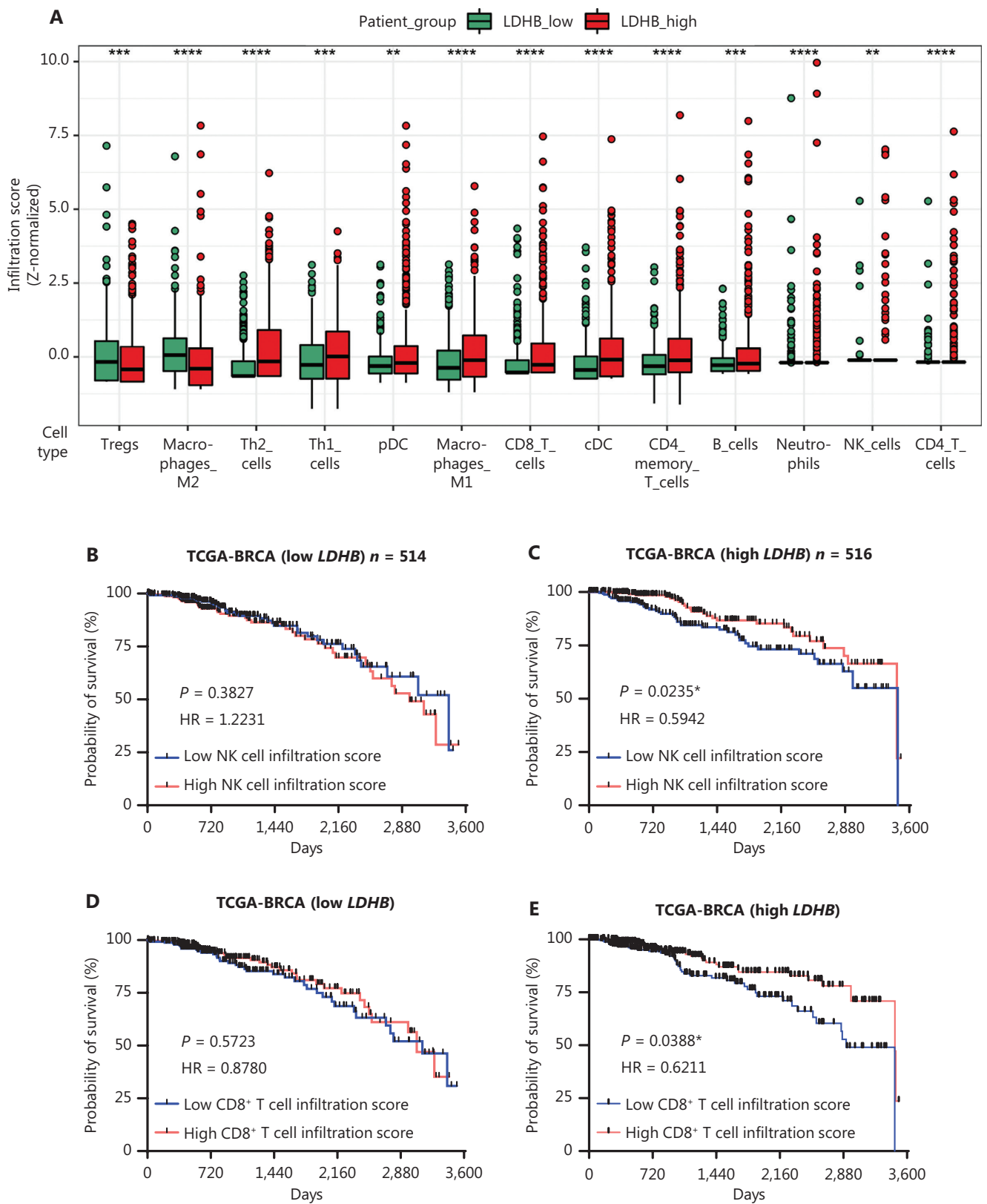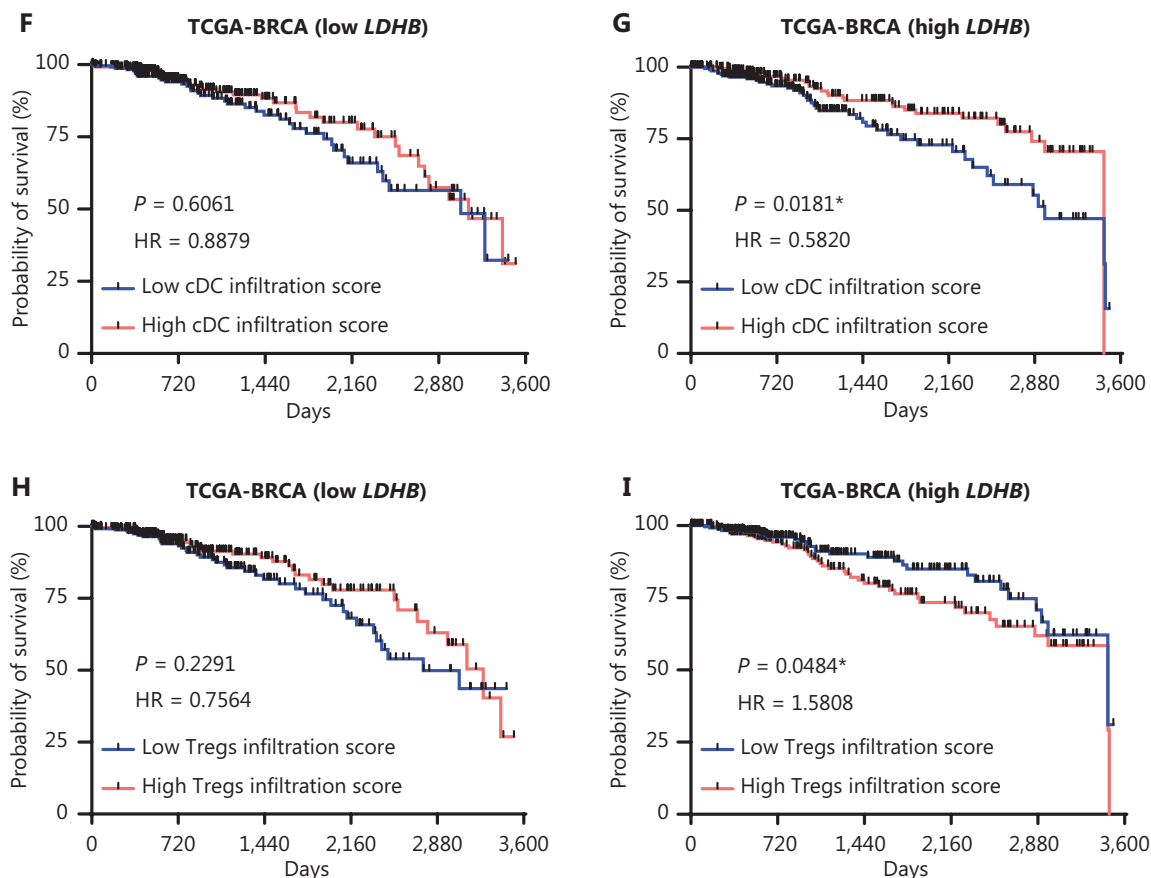
Figure 7 Continued

Figure 7 *LDHB* facilitates the formation of tumor immune-enhancing microenvironment in TCGA. (A) The distribution of 13 immune cell subset infiltration between the *LDHB* low and high groups. The immune infiltration assessment was performed using the xCell algorithm. (B-I) Kaplan-Meier analysis was performed to assess the correlation between immune cell infiltration and overall survival (OS) in breast cancer patients stratified by low and high *LDHB* expression. The survival plot displayed the status of four types of immune cells (B-I). The infiltration score median was used as the cut-off. Survival curves were plotted for patients with survival times < 3600 days. *P*-value was determined by the log-rank test (HR: hazard ratio) in all the analyses. *P*-value < 0.05 was considered significant (*P < 0.05, **P < 0.01, ***P < 0.001, ****P < 0.0001; "ns" indicates non-significance).

0.728, and 0.752 for BRCA, LIHC, and PAAD, respectively (**Figure 8E-G**). Moreover, Kaplan–Meier curves indicated that high levels of NK cell activation significantly prolong the lifespan of patients with high *LDHB* expression (BRCA: HR = 0.5818, P = 0.0180; LIHC: HR = 0.5157, P = 0.0037; PAAD: HR = 0.6043, P = 0.0944; **Figure 8H-M**). Therefore, our findings suggest that *LDHB* has good specificity and sensitivity for predicting NK cell activation in patients, and this model is potentially applicable to pan-carcinomas.

Discussion

Herein we evaluated immune infiltration patterns in patients by analyzing data from TCGA and clinical samples. Our results revealed that elevated *LDHB* expression is associated with improved NK cell-mediated cytotoxicity. Moreover, our findings demonstrated that *Ldhb* expression within tumors attenuates lactic acid secretion, thereby stimulating NK cells to impede tumor progression (**Figure 9**).

Previous studies have suggested that *LDHA* in melanoma cells impedes T and NK cell functions by promoting lactic acid secretion[23]. Similarly, our results revealed that *LDHA* hindered NK cell activity in BRCA cells (**Figure S6C**), demonstrating the high predictability and accuracy of our model. However, the role of *LDHB* in the immune microenvironment of BRCA has not been described. Our data demonstrated the presence of *LDHB* in BRCA-activated NK cells. TCGA and RNA-seq data from BRCA patients revealed that *LDHB* promotes

infiltration of T and NK cells. However, murine experiments did not reveal a significant effect of *Ldhb* on T and NK cell infiltration. We believe that differences may exist between subcutaneous mouse tumor models and the human tumor environment. Additionally, factors, such as the experimental time points and injection sites, could potentially influence the

infiltration of T and NK cells. In addition, we showed that *LDHB* gene expression serves as a reliable predictor of NK cell activity in BRCA, LIHC, and PAAD, highlighting the critical role in shaping the tumor immune microenvironment across multiple cancer types. Indeed, *LDHA* and *LDHB* have opposing functions in NK cell activation, which is consistent with
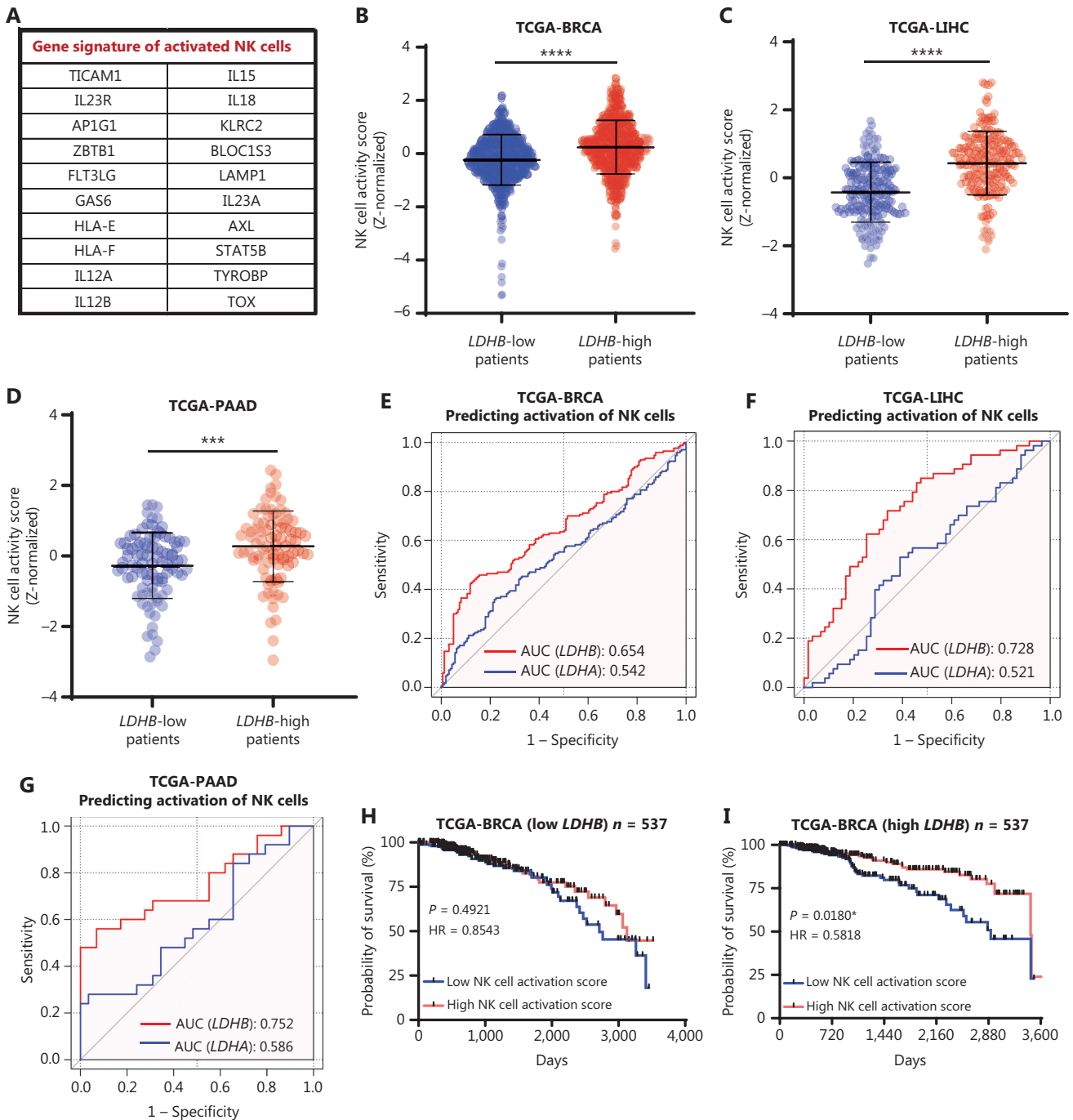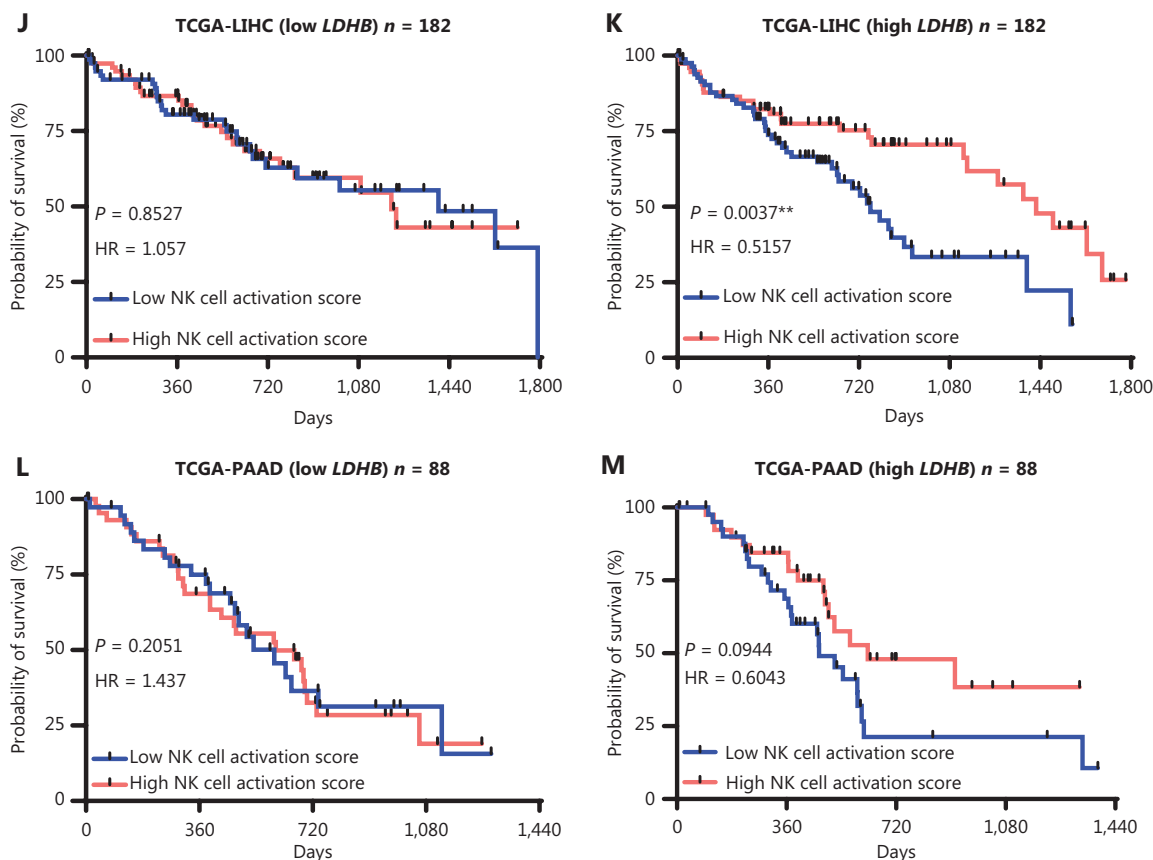

Figure 8   Continued

Figure 8 Clinical correlations with *LDHB* and NK cell activation in tumors. (A) The table showcases a list of gene sets associated with NK cell activation. (B-D) Single sample gene set enrichment analysis (ssGSEA) evaluated the signature of NK cell activity in patients. Patients with high and low *LDHB* expression were compared in groups. Data were collected from the TCGA database for breast cancer (BRCA) (B), liver cancer (LIHC) (C), and pancreatic cancer (PAAD) (D). NK cell activity score is calibrated by Z-normalized. (E-G) ROC curves of the *LDHB* expression to predict the NK cell activation in breast cancer (BRCA) (E), liver cancer (LIHC) (F), and pancreatic cancer (PAAD) (G) from TCGA. (H-M) Kaplan–Meier curve analysis of OS between the high NK cell activity score and low NK cell activity score in patients with different levels of *LDHB* expression. Data were collected from the TCGA database for breast cancer (BRCA) (H-I), liver cancer (LIHC) (J-K), and pancreatic cancer (PAAD) (L-M). Survival curves were plotted for patients with survival times < 3,600 days (BRCA), 1,800 days (LIHC), and 1,440 days (PAAD). In all the analyses, the results are expressed as the *mean ± SD*. *P*-values were calculated using a two-tailed unpaired t-test. *P* < 0.05 was considered significant (*P < 0.05, **P < 0.01, ***P < 0.001, ****P < 0.0001; "ns" indicates non-significance).

the respective roles in glycolysis. While *LDHA* promotes the conversion of pyruvate to lactic acid, *LDHB* tends to bind to lactic acid and convert lactic acid into pyruvate, thereby promoting the TCA[44]. In our subsequent analysis, we observed a significant positive correlation between *LDHB* and *MCT1* expression, indicating that *LDHB* eliminates intracellular lactic acid and absorbs excessive lactic acid from the TME, leading to the creation of an immune-promoting microenvironment. However, what was incomprehensible was the ability of *LDHB* to diminish lactate secretion while concurrently enhancing glucose uptake in 4T1 and BT-549 cells. Beyond pyruvate generation, glucose-derived metabolites

have a pivotal role in various biosynthetic pathways, such as nucleic acid and lipid synthesis[45]. Furthermore, LDHB facilitates the TCA cycle in 4T1 cells. This metabolic process in tumors exhibits a pronounced inclination toward lactate consumption[46]. Therefore, in the overexpressed *LDHB* cell lines, we hypothesized that increased *LDHB* levels lead to a pronounced surge in lactate absorption and utilization, thereby surpassing production. The Warburg effect is a well-known manifestation of metabolic reprogramming in tumor cells and is considered a key factor in the modulation of immune cells within the TME through metabolic substances[47-49]. A new aspect of this study was the link between immune cell
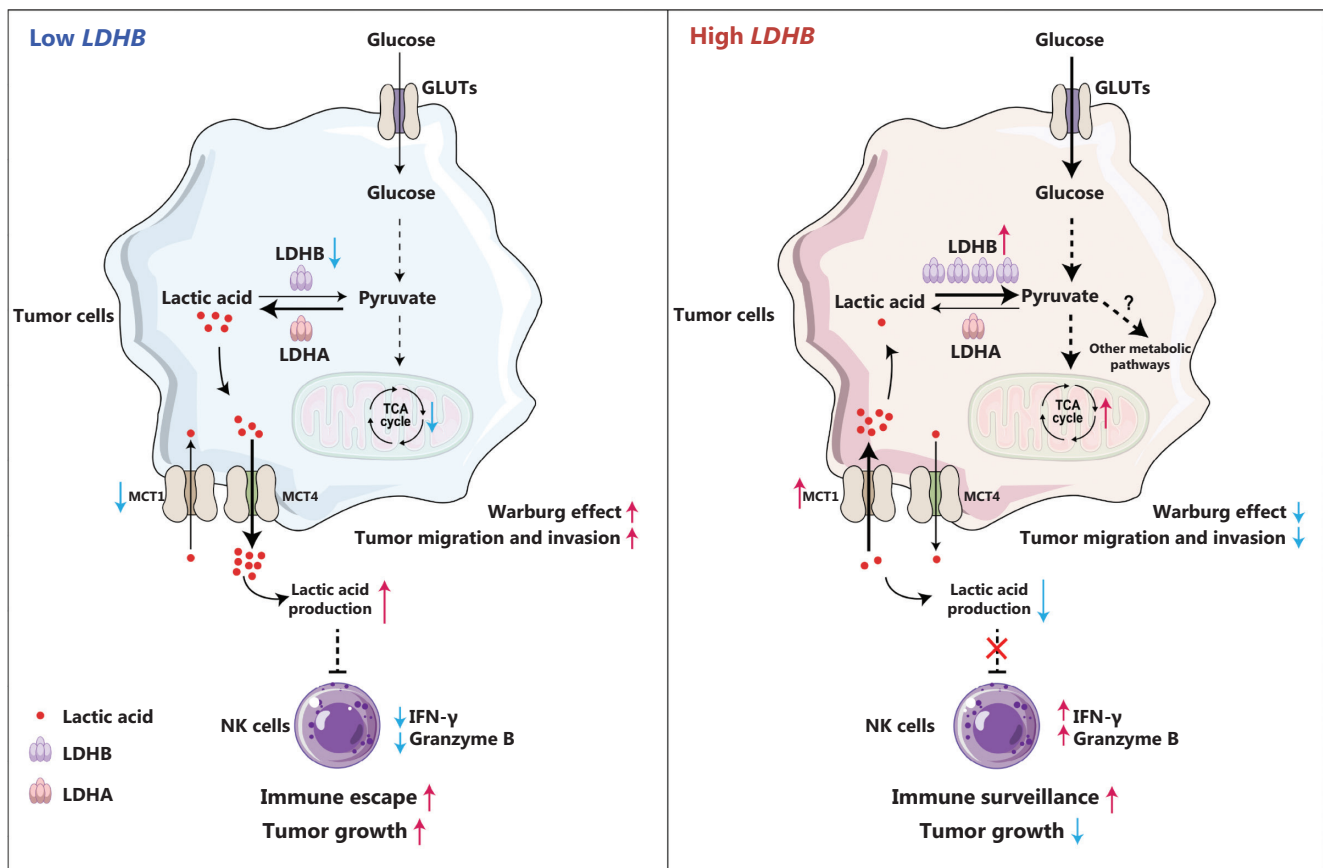
Figure 9 Working model: Metabolic and immune regulation by LDHB in breast cancer. The cellular metabolic conversion reaction between lactate and pyruvate is balanced by lactate dehydrogenase (LDH) A and B. When LDHB is downregulated, as frequently occurs in breast cancer, the reaction tends to be dominated by LDHA converting pyruvate to lactate that causes decreased tricarboxylic acid (TCA) cycles as well as increased secretion of the elevated intracellular lactate through MCT4, which is otherwise a relatively weak lactate exporter. Excess extracellular lactate may suppress NK cell activity, reduce IFN-γ and granzyme B production, and promote tumor immune escape. As a combined effect, tumor cells may exhibit an enhanced Warburg effect accompanied by increased growth, migration, and invasion. High LDHB, however, triggers a reverse conversion of lactate to pyruvate that should promote lactate import from extracellular environment through MCT1, which further releases NK cell activity and enhances immune surveillance. In addition, the TCA cycle and glucose uptake are upregulated, resulting in a diminished Warburg effect and suppressed tumor growth and metastasis.

activation, *LDHB* expression in tumor cells, and the Warburg effect in the TME.

Immune cells in the TME have a critical role in promoting or inhibiting tumor development. Macrophages are vital components of the TME[50]. While M1 macrophages hinder tumor development, M2 macrophages promote tumor progression[51,52]. Compared to M0 macrophages, M2 macrophages exhibit lower *LDHB* expression accompanied by elevated lactic acid secretion[53]. Our data suggest that BRCA *LDHB* affects the polarization of macrophages, promoting the polarization of M1 macrophages and inhibiting the polarization of M2 macrophages (**Figure 7A**). Similarly, lactic acid has been reported

to act directly as a signaling molecule. Tumor-derived lactic acid promotes the development of macrophages toward immunosuppression[54]. Moreover, our results revealed that tumor *LDHB* affects NK cell activity as well as activated CD8^{+} T cells, cDCs, and Tregs. Tregs are activated in modulated immune cells of patients with high *LDHB* expression. This finding indirectly suggests that immune cell activation is occasionally accompanied by Treg cell activation, which may be a significant factor contributing to the poor therapeutic efficacy of immunotherapy. Immunotherapy is effective only in patients with good immune infiltration[14,55]. Our results suggest that *LDHB* promoted activation of tumor-infiltrating NK cells and

26

Luo et al. Diminished *LDHB* in breast tumors impedes NK cells

infiltration of most immune cells, indicating that *LDHB* may convert "immune-cold" tumors to "immune-hot" tumors and improve the response of patients to immune checkpoint blockade therapy. Assessing *LDHB* expression in patients is promising for elucidating the immune microenvironment within tumors, potentially guiding clinical treatment decisions.

LDHB is frequently silenced by DNA methylation in prostate[56] and gastric cancers[57]. Additionally, low expression of *LDHB* promotes claudin-1-mediated invasion of hepatoma cells[58]. Consistent with these findings, our study demonstrated that overexpression of *LDHB* in BRCA cells significantly inhibits tumor cell migration and invasion. We propose that tumor invasion requires a significant amount of ATP to sustain the high-energy demand[59]. However, the reverse Warburg effect caused by *LDHB* impedes the rapid acquisition of ATP and intermediate metabolites by tumor cells, which consequently inhibits their migration and invasion. Moreover, the attenuation of tumor invasion may also be attributed to a reduction in lactic acid, which promotes tumor migration and invasion[44,60]. Therefore, our study provides evidence that *LDHB* overexpression inhibits tumor cell migration and invasion by disrupting the Warburg effect.

Although our study provides new insight into the role of *LDHB* in the regulation of immune responses in BRCA, some limitations should be noted. For example, use of the xCell algorithm to evaluate immune infiltration may not be completely accurate and the bulk transcriptome data from TCGA database may not fully represent the real expression of immune cells. Additionally, we proposed that lactic acid plays a crucial role in suppressing NK cell activation; however, additional investigations are required to determine whether other factors, such as cytokines or inflammatory factors, may also modulate NK cell function. Further experiments and extensive evidence are necessary to explore these possibilities and highlight the underlying mechanisms.

Conclusions

In summary, we demonstrated an association between *LDHB* and activation of tumor-infiltrating NK cells in BRCA. Our findings revealed that *LDHB* exerts an inverse Warburg effect, reducing lactic acid secretion, and promoting NK cell activation. Overall, our study suggests that *LDHB* may serve as a potential target for enhancing anti-tumor immune responses in patients with BRCA.

Grant support

Conflict of interest statement

No potential conflicts of interest are disclosed.

Author contributions

Conceived and designed the analysis: Zhihong Luo, Wenhua Li, Ke Gong.
Collected the data: Xiaohua Huang, Kefeng Wei, Xinyi Xu, Yi Zheng.
Contributed data or analysis tools: Zhihong Luo.
Performed the analysis: Zhihong Luo, Ke Gong.
Wrote the paper: Zhihong Luo, Wenhua Li.

Availability of data and material

The data generated in this study are available within the article and the supplementary data files.

Ethics approval and consent to participate

This study was approved by the Ethics Committee of the the University of Chinese Academy of Sciences-Shenzhen Hospital (Approval No. LL-KT-2022086).

References

1. Siegel RL, Miller KD, Wagle NS, Jemal A. Cancer statistics, 2023. CA Cancer J Clin. 2023; 73: 17-48.

2. Quail DF, Joyce JA. Microenvironmental regulation of tumor progression and metastasis. Nat Med. 2013; 19: 1423-37.

3. Zhuang X, Zhang H, Hu G. Cancer and microenvironment plasticity: double-edged swords in metastasis. Trends Pharmacol Sci. 2019; 40: 419-29.

4. Wang D, Wei H. Natural killer cells in tumor immunotherapy. Cancer Biol Med. 2023; 20: 539-44.

5. Mantovani A, Allavena P, Sica A, Balkwill F. Cancer-related inflammation. *Nature*. 2008; 454: 436-44.

6. Binnewies M, Roberts EW, Kersten K, Chan V, Fearon DF, Merad M, et al. Understanding the tumor immune microenvironment (time) for effective therapy. Nature Med. 2018; 24: 541-50.

7. Baginska J, Viry E, Paggetti J, Medves S, Berchem G, Moussay E, et al. The critical role of the tumor microenvironment in shaping natural killer cell-mediated anti-tumor immunity. Front Immunol. 2013; 4: 490.

8. Hasmim M, Messai Y, Ziani L, Thiery J, Bouhris JH, Noman MZ, et al. Critical role of tumor microenvironment in shaping NK cell functions: implication of hypoxic stress. Front Immunol. 2015; 6: 482.

9. Topalian SL, Drake CG, Pardoll DM. Immune checkpoint blockade: a common denominator approach to cancer therapy. Cancer Cell. 2015; 27: 450-61.

10. Alexandrescu DT, Ichim TE, Riordan NH, Marincola FM, Di Nardo A, Kabigting FD, et al. Immunotherapy for melanoma: current status and perspectives. J Immunother. 2010; 33: 570-90.

11. Wörmann SM, Diakopoulos KN, Lesina M, Algül H. The immune network in pancreatic cancer development and progression. Oncogene. 2014; 33: 2956-67.

12. Song X, Zhou Z, Li H, Xue Y, Lu X, Bahar I, et al. Pharmacologic suppression of B7-H4 glycosylation restores antitumor immunity in immune-cold breast cancers. Cancer Discov. 2020; 10: 1872-93.

13. Goldberg J, Pastorello RG, Vallius T, Davis J, Cui YX, Agudo J, et al. The immunology of hormone receptor positive breast cancer. Front Immunol. 2021; 12: 674192.

14. Tumeh PC, Harview CL, Yearley JH, Shintaku IP, Taylor EJ, Robert L, et al. PD-1 blockade induces responses by inhibiting adaptive immune resistance. Nature. 2014; 515: 568-71.

15. Cristescu R, Mogg R, Ayers M, Albright A, Murphy E, Yearley J, et al. Pan-tumor genomic biomarkers for PD-1 checkpoint blockade-based immunotherapy. Science. 2018; 362: eaar3593.

16. Hiam-Galvez KJ, Allen BM, Spitzer MH. Systemic immunity in cancer. Nat Rev Cancer. 2021; 21: 345-59.

17. Rodig SJ, Gusenleitner D, Jackson DG, Gjini E, Giobbie-Hurder A, Jin C, et al. MHC proteins confer differential sensitivity to CTLA-4 and PD-1 blockade in untreated metastatic melanoma. Sci Transl Med. 2018; 10: eaar3342.

18. Lanier LL. NK cell recognition. Ann Rev Immunol. 2005; 23: 225-74.

19. Kärre K. Natural killer cell recognition of missing self. Nat Immunol. 2008; 9: 477-80.

20. Ardolino M, Azimi CS, Iannello A, Trevino TN, Horan L, Zhang L, et al. Cytokine therapy reverses NK cell anergy in MHC-deficient tumors. J Clin Invest. 2014; 124: 4781-94.

21. Li X, Wenes M, Romero P, Huang SC, Fendt SM, Ho PC. Navigating metabolic pathways to enhance antitumour immunity and immunotherapy. Nat Rev Clin Oncol. 2019; 16: 425-41.

22. He X, Lin H, Yuan L, Li B. Combination therapy with L-arginine and α-PD-l1 antibody boosts immune response against osteosarcoma in immunocompetent mice. Cancer Biol Ther. 2017; 18: 94-100.

23. Brand A, Singer K, Koehl GE, Kolitzus M, Schoenhammer G, Thiel A, et al. LDHA-associated lactic acid production blunts tumor immunosurveillance by T and NK cells. Cell Metab. 2016; 24: 657-71.

24. Hanahan D, Weinberg RA. Hallmarks of cancer: the next generation. Cell. 2011; 144: 646-74.

25. Hsu PP, Sabatini DM. Cancer cell metabolism: Warburg and beyond. Cell 2008; 134: 703-7.

26. Vander Heiden MG, Cantley LC, Thompson CB. Understanding the warburg effect: the metabolic requirements of cell proliferation. Science. 2009; 324: 1029-33.

27. Urbańska K, Orzechowski A. Unappreciated role of LDHA and LDHB to control apoptosis and autophagy in tumor cells. Int J Mol Sci. 2019; 20: 2085.

28. Quistorff B, Secher NH, Van Lieshout JJ. Lactate fuels the human brain during exercise. FASEB J. 2008; 22: 3443-9.

29. Wang T, Chen K, Yao W, Zheng R, He Q, Xia J, et al. Acetylation of lactate dehydrogenase B drives NAFLD progression by impairing lactate clearance. J Hepatol. 2021; 74: 1038-52.

30. Mishra D, Banerjee D. Lactate dehydrogenases as metabolic links between tumor and stroma in the tumor microenvironment. Cancers. 2019; 11: 750.

31. Ždralević M, Brand A, Di Ianni L, Dettmer K, Reinders J, Singer K, et al. Double genetic disruption of lactate dehydrogenases A and B is required to ablate the "warburg effect" restricting tumor growth to oxidative metabolism. J Biol Chem. 2018; 293: 15947-61.

32. McCleland ML, Adler AS, Shang Y, Hunsaker T, Truong T, Peterson D, et al. An integrated genomic screen identifies LDHB as an essential gene for triple-negative breast cancer. Cancer Res 2012; 72: 5812-23.

33. Eales KL, Hollinshead KE, Tennant DA. Hypoxia and metabolic adaptation of cancer cells. Oncogenesis 2016; 5: e190.

34. Yu G, Wang LG, Han Y, He QY. clusterProfiler: an R package for comparing biological themes among gene clusters. OMICS. 2012; 16: 284-7.

35. Aran D, Hu Z, Butte AJ. xcell: digitally portraying the tissue cellular heterogeneity landscape. Genome Biol. 2017; 18: 220.

36. Hänzelmann S, Castelo R, Guinney J. GSVA: Gene set variation analysis for microarray and RNA-seq data. BMC Bioinformatics. 2013; 14: 7.

37. Fan Y, Jiang S, Hua M, Feng S, Feng M, Wang R. Machine learning-based radiomics predicts radiotherapeutic response in patients with acromegaly. Front Endocrinol. 2019; 10: 588.

38. Yuan M, Breitkopf SB, Yang X, Asara JM. A positive/negative ion-switching, targeted mass spectrometry-based metabolomics

platform for bodily fluids, cells, and fresh and fixed tissue. Nat Protoc. 2012; 7: 872-81.

39. Abu-Hanna J, Patel JA, Anastasakis E, Cohen R, Clapp LH, Loizidou M, et al. Therapeutic potential of inhibiting histone 3 lysine 27 demethylases: a review of the literature. Clin Epigenetics. 2022; 14: 98.

40. Simonetta F, Alvarez M, Negrin RS. Natural killer cells in graft-versus-host-disease after allogeneic hematopoietic cell transplantation. Front Immunol. 2017; 8: 465.

41. Gallo M, Sapio L, Spina A, Naviglio D, Calogero A, Naviglio S. Lactic dehydrogenase and cancer: an overview. Front Biosci. 2015; 20: 1234-49.

42. Halestrap AP. The SLC16 gene family - structure, role and regulation in health and disease. Mol Aspects Med. 2013; 34: 337-49.

43. Doherty JR, Cleveland JL. Targeting lactate metabolism for cancer therapeutics. J Clin Invest. 2013; 123: 3685-92.

44. Goetze K, Walenta S, Ksiazkiewicz M, Kunz-Schughart LA, Mueller-Klieser W. Lactate enhances motility of tumor cells and inhibits monocyte migration and cytokine release. Int J Oncol. 2011; 39: 453-63.

45. Caro P, Kishan AU, Norberg E, Stanley IA, Chapuy B, Ficarro SB, et al. Metabolic signatures uncover distinct targets in molecular subsets of diffuse large B cell lymphoma. Cancer Cell. 2012; 22: 547-60.

46. Faubert B, Li KY, Cai L, Hensley CT, Kim J, Zacharias LG, et al. Lactate metabolism in human lung tumors. Cell. 2017; 171: 358-71.e9.

47. Pilon-Thomas S, Kodumudi KN, El-Kenawi AE, Russell S, Weber AM, Luddy K, et al. Neutralization of tumor acidity improves antitumor responses to immunotherapy. Cancer Res. 2016; 76: 1381-90.

48. Cascone T, McKenzie JA, Mbofung RM, Punt S, Wang Z, Xu C, et al. Increased tumor glycolysis characterizes immune resistance to adoptive T cell therapy. Cell Metab. 2018; 27: 977-87.e4.

49. Singer K, Kastenberger M, Gottfried E, Hammerschmied CG, Büttner M, Aigner M, et al. Warburg phenotype in renal cell carcinoma: high expression of glucose-transporter 1 (GLUT-1) correlates with low CD8(+) T-cell infiltration in the tumor. Int J Cancer. 2011; 128: 2085-95.

50. Ge Z, Ding S. The crosstalk between tumor-associated macrophages (TAMs) and tumor cells and the corresponding targeted therapy. Front Oncol. 2020; 10: 590941.

51. Larionova I, Tuguzbaeva G, Ponomaryova A, Stakheyeva M, Cherdyntseva N, Pavlov V, et al. Tumor-associated macrophages in human breast, colorectal, lung, ovarian and prostate cancers. Front Oncol. 2020; 10: 566511.

52. Chen Y, Song Y, Du W, Gong L, Chang H, Zou Z. Tumor-associated macrophages: an accomplice in solid tumor progression. J Biomed Sci. 2019; 26: 78.

53. Frank AC, Raue R, Fuhrmann DC, Sirait-Fischer E, Reuse C, Weigert A, et al. Lactate dehydrogenase B regulates macrophage metabolism in the tumor microenvironment. Theranostics 2021; 11: 7570-88.

54. Hutcheson J, Balaji U, Porembka MR, Wachsmann MB, McCue PA, Knudsen ES, et al. Immunologic and metabolic features of pancreatic ductal adenocarcinoma define prognostic subtypes of disease. Clin Cancer Res. 2016; 22: 3606-17.

55. Semiglazov V, Tseluiko A, Kudaybergenova A, Artemyeva A, Krivorotko P, Donskih R. Immunology and immunotherapy in breast cancer. Cancer Biol Med. 2022; 19: 609-18.

56. Leiblich A, Cross SS, Catto JW, Phillips JT, Leung HY, Hamdy FC, et al. Lactate dehydrogenase-B is silenced by promoter hypermethylation in human prostate cancer. Oncogene. 2006; 25: 2953-60.

57. Maekawa M, Taniguchi T, Ishikawa J, Sugimura H, Sugano K, Kanno T. Promoter hypermethylation in cancer silences LDHB, eliminating lactate dehydrogenase isoenzymes 1-4. Clin Chem. 2003; 49: 1518-20.

58. Kim JH, Kim EL, Lee YK, Park CB, Kim BW, Wang HJ, et al. Decreased lactate dehydrogenase B expression enhances claudin 1-mediated hepatoma cell invasiveness via mitochondrial defects. Exp Cell Res. 2011; 317: 1108-18.

59. Bartman CR, Weilandt DR, Shen Y, Lee WD, Han Y, TeSlaa T, et al. Slow TCA flux and ATP production in primary solid tumours but not metastases. Nature. 2023; 614: 349-357.

60. Webb BA, Chimenti M, Jacobson MP, Barber DL. Dysregulated pH: a perfect storm for cancer progression. Nat Rev Cancer. 2011; 11: 671-7.